Chemical Analysis of Sediments Using X-Ray Fluorescence On-board an Autonomous Underwater Vehicle

Jeremy Peter Breen, Dip. Langs, B. Comp. (Hons) - B. Sc.

Submitted in fulfilment of the requirements for the degree of
Doctor of Philosophy
University of Tasmania

August, 2013

Contents

List of Figures

List of Tables

Declaration of Originality

This thesis contains no material which has been accepted for a degree or diploma by the University or any other institution, except by way of background information and duly acknowledged in the thesis, and to the best of my knowledge and belief no material previously published or written by another person except where due acknowledgement is made in the text of the thesis, nor does the thesis contain any material that infringes copyright.

Date:

Authority of Access

Date:

Statement of Co-authorship

The following are publications of work undertaken as part of this thesis:

[1] **Breen, J., de Souza, P., Timms, G., Ollington, R., 'Onboard assessment of XRF spectra using genetic algorithms for decision making on an autonomous underwater vehicle', Nuclear Instruments and Methods in Physics Research Section B: Beam Interactions with Materials and Atoms, Volume 269, Issue 12, 15 June 2011, Pages 1341-1345**

J.Breen (60%) and P. de Souza (20%) were the main authors. J. Breen was primarily responsible for algorithm development, implementation and subsequent data analysis with P. de Souza assisting with conception. G. Timms (10%) also provided significant contribution to the manuscript. R. Ollington (10%) provided assistance with algorithm development and manuscript editing.

[2] **Breen, J., de Souza, P., Timms, G., McCulloch, J., Ollington, R. B., 'Analysis of Heavy Metals in Marine Sediment using a Portable X-ray Fluorescence Spectrometer Onboard an Autonomous Underwater Vehicle', Proceedings - Oceans 2012, 21-24 May 2012, Yeosu, Korea**

J. Breen was the primary author (65%). He performed the majority of the experimental work and subsequent analysis. P. de Souza (10%) assisted with the analysis . G. Timms (10%) assisted with setting up the experimen-

tal system and J. McCulloch (10%) designed the electronic component of the underwater housing discussed in the paper. R. Ollington (5%) provided general support and advice. All authors provided feedback and suggestions on the manuscript.

[3]**Breen, J., de Souza, P.A., Timms, G.P., Ollington, R., 'Adaptive behaviour for an Autonomous Underwater Vehicle to perform chemical mappings', Proceedings - Oceans 2010, 24-27 May 2010 , Sydney, Australia**

J. Breen was the primary author (70%). He performed the majority of the experimental work and subsequent analysis. P. de Souza (10%), G. Timms (10%) and R. Ollington (10%) provided general support and advice. All authors provided feedback and suggestions on the manuscript.

We the undersigned agree with the above stated proportion of work undertaken for each of the above published manuscripts contributing to this thesis.

Jeremy Breen (Candidate)
Date:

Dr. Robert Ollington (Primary Supervisor)
Date:

Abstract

Advances in robotics have led to the development of autonomous platforms capable of exploring regions that are inaccessible for humans. These regions range from extra-terrestrial surfaces, such as Mars and Titan, to the bottom of our oceans. In addition to robotics there have also been advances in sensor technologies in areas such as power consumption, size, weight, and communications. The combination of field robotics with novel sensing capabilities provides exciting science opportunities. Autonomous measurement of phenomena present in the environment offers an alternative to expensive, time-consuming manual measurements.

This thesis investigates the novel use of a miniaturised X-Ray Fluorescence (XRF) spectrometer sensor system as part of the scientific payload on an Autonomous Underwater Vehicle (AUV). This will allow the automated in situ semi-quantitative analysis of heavy metal contamination present in marine sediments. Heavy metal contamination of sediments is particularly important because of its potential impact on associated ecosystems and human health.

To achieve this capability the XRF system has been integrated with the AUV using a custom housing that enables the sensor to be operated safely underwater. A landing behaviour has been developed for the AUV that enables the vehicle to land on the seabed, without significantly disturbing the sediment layer, and to then remain in a stationary position for the duration of the measurement. Automated data analysis using genetic algorithms was performed on the XRF data on-board the vehicle. This would enable the AUV control system to make informed decisions based on the results of measurements facilitating adaptive sampling strategies.

A total of 21 in situ measurements have been performed in the Derwent estuary region, located in south-east Tasmania, Australia. The results show significantly higher relative heavy metal concentrations in areas of industrial activity. This demonstrates the developed system can perform in situ

measurements that can be used to observe spatial variations in heavy metal contamination. The resulting data from these measurements can guide further comprehensive environmental monitoring missions by supporting site selection or assisting with the remediation of contaminated sediments.

The research contribution presented in this thesis has been the development of the capability to autonomously and intelligently perform in situ measurements and data analysis of marine sediments using an AUV equipped with a miniaturised XRF spectrometer. The next stage of this research will aim to increase the scientific return of measurement missions by the real-time inclusion of scientific sensor data in decision-making processes to enable adaptive sampling.

Acknowledgements

I have been lucky enough to have three great supervisors in Dr. Paulo de Souza, Dr. Robert Ollington and Dr. Greg Timms. Their support and guidance throughout my candidature has been invaluable. They have shown an enthusiasm for performing novel, innovative research that has proven contagious and encouraged me to challenge myself throughout. I have learned a great deal from their shared knowledge and experience which has aided me in developing my skills and preparing for future challenges. I would also like to extend my gratitude to my former supervisor Dr. Ray Williams for his help during the formative stages of my research and ongoing advice. This research would not have been possible without the support provided by the CSIRO ICT Centre's Intelligent Sensing and Systems Laboratory (ISSL), where I have spent a large portion of time. They provided funding, infrastructure and support throughout my candidature. The staff also made me feel welcome and part of the lab. In particular I would like to acknowledge the following individuals. Andrew 'Boo' Davie has provided me with great assistance. He has assisted me with all field work associated with this thesis and provided suggestions and an alternate view on problems encountered. His knowledge and expertise with the Starbug AUV were invaluable. He also provided feedback on my thesis. John McCulloch helped significantly with the design of the electronics for the spectrometer housing as well as providing valuable assistance and support with my work and the AUV platform. Chris Sharman managed the project that my research was a part of and provided me with the necessary support required. Trevor Goodwin, from the CSIRO's Climate and Atmospheric Research (CMAR) laboratory, built the electronics required to operate the XRF system on-board the AUV and

provided ongoing support and advice on the implementation. Tony Sprent built the majority of the XRF system housing. The CSIRO's Autonomous Systems Laboratory (ASLab), in particular Matt Dunbabin, for the initial development of the Starbug AUV platform and ongoing support. The lab also worked on initial development of the AUV simulator that I used in my research. The Australian Research Council Centre of Excellence in Ore Deposits for supplying the sediment samples, in particular Dan Gregory. The University of Tasmania and the CSIRO ICT centre for providing me with an Australian Postgraduate Award (APA) scholarship and top up scholarship respectively. This allowed me to complete my PhD as a full time student. My friends and family for providing their support and understanding throughout my PhD. My parents especially have been very supportive throughout my schooling, nurturing my enthusiasm for science and I owe them a great deal. My fellow PhD student, Chris Jackett, for his friendship and accompanying me throughout this experience. Finally my girlfriend Renee. I am eternally grateful for her love and support throughout my time as a PhD student.

Chapter 1

Introduction

The ability to monitor and sense an ever changing world is crucial for understanding various processes and phenomena. This can provide knowledge of how human actions impact the environment. Advancements in sensing related technologies create opportunities to sense the world in new and exciting ways.

Scientific observations are sometimes required to be performed at places considered to be inaccessible or unsafe for human beings. These places might be on another planet, inside and around an active volcano or deep under our oceans. Advances in robotics have led to the development of autonomous platforms that are capable of exploring these and other hostile regions (Bellingham and Rajan 2007). Examples of such platforms include robotic rovers that have been sent to Mars (Squyres et al. 2009), exploring an active volcano, Mount Erebus, in Antarctica (Wettergreen et al. 1993) and in radioactive environments (Iborra et al. 2003).

The monitoring and management of marine resources is a challenging task. For example the creation of giant marine reserves require extensive monitoring to detect any potentially damaging changes within the environment (Pala 2013). These monitoring tasks can be facilitated through the development of various machines which can be deployed with sensors to perform measurements in hazardous places (e.g., deep sea or cold waters), for extensive period of times (e.g., beyond those safe for divers) and at rela-

tively low cost. Examples of these machines include gliders, Argo floats, Autonomous Underwater Vehicles (AUVs), and Remotely Operated Vehicles (ROVs) (Yuh and West 2001; Schofield et al. 2007; Gould et al. 2004). AUVs have been increasingly used in a variety of scientific, industrial and military applications due to their ability to be deployed untethered and operate without direct human supervision. They provide a platform for attaching a wide range of scientific and engineering sensors that allows them to explore the marine environment. The range of phenomenon able to be monitored by these platforms is increasing due to improvements in sensing technologies, such as miniaturisation. This provides interesting research opportunities in the area of autonomous monitoring of marine environments.

This thesis investigates the novel use of a miniaturised X-Ray Fluorescence (XRF) spectrometer sensor system as part of the scientific payload on an AUV. This allows the automated, in situ and semi-quantitative analysis of heavy metal contamination present in marine sediments.

1.1 Motivation

This section discusses the motivation for performing in situ automated sampling of marine sediment using an AUV. The target area for the field work is the Derwent Estuary in south-east Tasmania, Australia. The Derwent Estuary is a focal part of Hobart's metropolitan centre with 40% of the population of Tasmania living around its shores. It supports a wide range of commercial, industrial, recreational and social uses and, resulting from its intense use, faces a variety of environmental pressures. These include infestation by introduced species such as the northern Pacific sea-star, loss of native habitats and species, elevated levels of nutrients and organic material, and heavy metal contamination of the water, sediments and seafood (Whitehead et al. 2009; Butler 2006). To maintain the health of the estuary it is vital that adequate monitoring regimes are in place. Contamination by heavy metals is one of the main issues facing the Derwent Estuary.

Heavy metal pollutants are introduced into the water through a variety of sources, and eventually settle onto the seabed. These potential sources

include long-term industrial activity, urban runoff, air pollution and refuse sites. Contaminants can have toxic effects on the marine ecosystem, through bio-accumulation of metals occurring in organisms exposed to the sediment, and can work their way through the food chain to human consumption (Ansari et al. 2004). There has been significant research investigating the scope of heavy metal contamination in the Derwent Estuary. The concentrations of zinc , mercury, cadmium, lead, copper and arsenic all exceed national sediment quality guidelines making the Derwent Estuary one of the most polluted estuaries in terms of heavy metal contamination in the world (Bloom and Ayling 1977; Butler 2006; and references therein).

Regular monitoring of heavy metals in the sediment is important for mitigating against their potentially harmful effect and remediation of contaminated areas. Current techniques used to sample sediments require manual processes. Samples are commonly taken using either a grab or core sampler (EPA 2003). However there are certain disadvantages associated with these techniques.

- They require the use of large support vessels, potentially equipped with cranes, in order to deploy the sampling mechanisms. This can be expensive, both financially and in terms of other resources such as labor.

- The process of taking a measurement can disturb the surface layer of sediments, which is the most bio-available to marine organisms and therefore the most relevant to the health of the environment. This makes it difficult to obtain a clear indication of the level of contamination in surface sediments.

- Once a sample has been taken it then undergoes elemental analysis which requires the extraction and preparation of the sample followed by laboratory work. This creates a significant delay between the collection of samples and subsequent analytical processes. This lack of immediate feedback on the composition of the sample makes it difficult to adaptively change sampling strategy in the field in response to the discovery of regions of interest (i.e. hotspots of heavy metals) or to react quickly to potentially dangerous levels of contamination.

The possibility of developing an alternate technique that addresses these issues presents a unique research challenge and opportunity. A suitable technique would have the following characteristics.

- The ability to perform in situ measurements. This removes the need to take physical samples, reducing the disturbance caused to the surface sediments. Instead instrumentation can be placed in direct contact with the surface sediment layer.
- Measurements to be performed in an autonomous manner. This would involve a type of robotic platform that can operate underwater without direct human supervision, reducing costs associated with the measurement.
- Autonomous data analysis capability can allow the sensed information to be processed in real-time on-board the robotic platform. This allows the results of measurements to be available immediately providing the potential for adaptively controlling the vehicle based on collected data.

1.2 Research Objectives

The main objective of this thesis is the development and implementation of a novel sampling technique for marine sediments. This technique is the in situ analysis of sediments using a miniaturised X-Ray Fluorescence spectrometer that has been attached to an AUV. The hypothesis of this research is that the technique will be capable of detecting spatial variability in heavy metal concentrations in measurements performed in the Derwent Estuary. This allows for the identification of contamination hotspots within the sampled region. The following comprises the main research components that will be discussed throughout this thesis:

1. The XRF system, comprising of an X-ray spectrometer and X-ray tube, and how it has been integrated with the AUV platform.
2. The development of the automated data analysis algorithm that can be performed on the AUV immediately after the analysis.

3. The AUV is required to land on the seafloor in order to perform the measurements. This involves navigating to landing on a predetermined location. The vehicle needs to be identified as landing before a measurement can commence. During the measurement the AUV's state will need to be recorded to assess if it moved significantly. If the vehicle was not stationary it may impact on the quality of the recorded data.

This work provides the framework for the future implementation of an adaptive sampling strategy. This will increase the scientific return of sampling missions through enabling the robotic platform to make decisions on subsequent measurement sites based on data it has acquired. These decisions could be to increase the sampling resolution around regions of interest, where high levels of heavy metals have been detected.

1.3 Thesis Structure

Chapter 2 discusses the topic of AUVs. Some existing platforms and some of their applications are mentioned. The AUV that will be used for the research, called Starbug, will be introduced. This will be done through presenting its capabilities, a description of sensor payloads and previous work.

The automated data analysis of XRF spectra is discussed in Chapter 3. A brief background of the technique of XRF spectroscopy is given. Some existing applications are also discussed, including those related to the analysis of marine sediments. A method using genetic algorithms is proposed that will allow the unsupervised curve fitting of spectral data to provide a semi-quantitative analysis of elemental concentrations. This can be implemented on the AUV platform for analysis in real-time, that can then be used to drive future work on developing adaptive sampling approaches.

The AUV will be required to perform various actions within its environment necessary to performing the measurements. These are discussed in Chapter 4. This includes the work that has been done on landing the AUV on the seabed and the process of performing measurements. Also included

in this chapter is a discussion on the process of integrating the XRF system with the AUV. This involves the development of a suitable housing to allow the device to be operated and controlled underwater by the AUV computer.

Results from measurements conducted are presented and discussed in Chapter 5, including experiments done in the laboratory as well as in situ sampling performed in the Derwent estuary.

A conclusion to this research is given in Chapter 6. This reinforces the significance of this work, as well as mentioning the limitations of the technique and possible areas of future research.

Chapter 2

Autonomous Underwater Vehicles

2.1 Introduction

Autonomous Underwater Vehicles (AUVs) are increasingly being seen as an important tool for both scientific and military applications. This is because of their ability to operate untethered, without direct human supervision at low cost and with a small number of operators. The majority of AUVs are between 1.5 and 6 metres long with a weight of anywhere from under 50kg to over 2 tons (Hagen et al. 2008). There are a wide range of sensors which AUVs can be equipped with, including sonar, echo sounders, video and still cameras, magnetometers and spectrometers. This chapter discusses the development and applications of some AUVs. The AUV that was used for this research, the Starbug platform, will be introduced.

2.2 AUV Technology

The underwater environment presents unique challenges to the development of AUVs. AUVs have to operate with limited resources, such as power and time available to execute a mission. The technology involved with underwater robotic platforms needs to be robust enough to maximise the scientific return

of missions performed.

One key technological component is the navigation and localisation of an AUV. While on the surface GPS can be used. However, once underwater the GPS signal is attenuated and alternative methods are required. The underwater environment does not allow passage of GPS signals. Having an accurate method of tracking the vehicle's location underwater is important for spatially correlating measurements taken.

The simplest approach to navigating underwater is to use dead reckoning (An 2003). This involves integrating the vehicle's velocity over time to give an approximation for its current location. A compass is used to determine heading, while an Inertial Measurement Unit (IMU) measures velocity as well as pitch, roll and yaw. However this method of navigation fails to take into account the velocity component attributed to ocean current. This problem can be solved through the use of a Doppler Velocity Log (DVL) sonar. This involves transmitting an acoustic ping which is reflected off the seafloor. The Doppler shift in the reflected signal can be used to calculate the real vehicle velocity relative to the seafloor. An alternate approach is to make use of the strong propagation characteristics of acoustic signals through the ocean environment. This is done by deploying acoustic beacons at known locations in the AUV's operating area (Matos et al. 1999). The most accurate implementation of this idea is known as the Long Baseline (LBL) system. The AUV can ping the acoustic beacons which then return the signal. The time taken for the AUV to receive the response can then be used to triangulate its position. Another method involves using geophysical navigation (Stutters et al. 2008). This technique is based on using features of the surrounding environment for localisation. These features may be known a priori from maps, or discovered during the duration of a mission. The use of Simultaneous Localisation And Mapping (SLAM) is also a popular technique for navigation (West and Syrmos 2006). This relies on the vehicle building a map of the underwater environment and tracking its location within this map. Features from the environment are extracted and tracked, and the vehicle's position relative to these features can be determined.

Another area of importance involves communication with the vehicle.

This may be done with a Wi-Fi connection while on the surface. However, issues are again encountered once the vehicle submerges. Underwater communication generally utilises acoustic transmission because of the poor transmission of radio waves under water (Stojanovic 1996). Acoustic communications can work well in the deep ocean but fall into difficulty when used in shallow, estuarine or coastal regions where multiple reflections can reduce the signal-to-noise ratio (SNR) and, hence, reduce effective data rates (Zielinski et al. 1995). The transmission of repeated detailed images, XRF spectra or optical data is not feasible under these conditions. However, there have been a number of AUVs which have communication capabilities while underwater. One example is using an acoustic modem with an AUV to gain a data-rate of 5000 bps at a 6 kilometre range (Singh et al. 2009). Communication capabilities is especially important when dealing with AUVs that perform under-ice exploration (King et al. 2010). This allows for localisation of the vehicle which aids in recovery. This prevents expensive platforms becoming lost in the difficult environments.

For the majority of vehicles, once they are submerged they no longer have communication with a human operator. This means they need to be able to make autonomous decisions in order to adapt to their environment. Therefore performing intelligent operations with AUVs is an active research area.

2.3 Intelligent Sampling with AUVs

In order to increase the scientific return of AUV missions, there has been research done on performing measurements in an adaptive fashion. Under normal operations, AUVs follow a pre-determined mission plan which involves sampling at pre-selected locations. There is a clear distinction between engineering and scientific sensors. Data collected by scientific sensors are normally used for post-mission processing, while engineering sensors are utilised in real-time for AUV operation (Robinson et al. 2010). To fully realise the scientific potential of advanced sensors on-board AUVs, data from the scientific sensors needs to be integrated into the control of the AUV in

real-time. Using an adaptive sampling paradigm the AUV can process collected scientific data on-board and adapt its sampling strategies accordingly. This approach is shown through the investigation of chemical concentrations in the water column (Camilli et al. 2004). When a mission was undertaken that relied on a sampling strategy and mission plan that were devised a priori it was found that regions of little interest were over sampled while in other regions with high variability the sampling resolution was inadequate. They propose the implementation of threshold values that trigger an adaptive sampling behaviour. An example given is an AUV sampling using a square box pattern until it encounters a chemical concentration higher than a certain value. It then starts sampling in a grid type pattern, providing higher sampling resolution. These trigger thresholds may be static values, or rely on the rate of change of concentration. A similar example is the adaptive tracking of thermoclines (Cruz and Matos 2010). An AUV performs a standard yo-yo (descending and ascending in a sinusoidal manner) until it detects a vertical temperature gradient above a given threshold. At this stage the vehicle will attempt to manoeuvre vertically within the constraints of the thermocline layer. Adaptive sampling can also be beneficial for the tracing of chemical plumes to a source location (Farrell, Pang, Li and Arrieta 2003). The approach used here is similar to odour-guided behaviour demonstrated by several animal species.

Another approach to adaptive sampling using AUVs is to use multiple vehicles to sample the environment in an efficient and collaborative manner (Leonard et al. 2010; Popa et al. 2004). Multiple vehicles can act as an autonomous, mobile sampling network acting cooperatively to minimise the uncertainty in measurements.

A novel use of adaptive sampling with AUVs uses several water samplers which can be triggered to take samples when particular criteria are satisfied (Zhang et al. 2010). An adaptive triggering algorithm is presented which collects a water sample when a chlorophyll fluorescence peak is detected.

2.4 AUV Platforms

There have been many AUV platforms developed by a range of organisations. The exploration of deep sea environments, which is potentially dangerous for humans, is a particularly active area of research.

The underwater vehicle Nereus, developed by the Woods Hole Oceanographic Institution (WHOI), has been designed to perform scientific measurements and sampling at depths of 11,000 metres (Bowen et al. 2008). It is able to be operated in two modes, as an AUV platform and also as an ROV via a fibre optic tether. The vehicle has to be able to withstand the immense pressure experienced at depth requiring it to be solidly built, weighing 2,800 kg. WHOI have also developed an AUV, SeaBed, which is capable of slowly moving or hovering over the seafloor at depths of up to 2,000 metres. This vehicle is designed to obtain high resolution sonar and optical images of the seafloor. The Monterey Bay Aquarium Research Institute (MBARI) has developed a similar torpedo shape vehicle called the Dorado (Kirkwood 2007; Thompson 2007). The length of these vehicles range from 3 to over 5 metres with a weight of between 476 kg and 635 kg. This heavy weight necessitates the use of a crane aboard a large vessel for deployment and retrieval. The Dorado Class AUV is predominately used for two main applications. These are to perform high resolution mapping of the seabed and to measure characteristics of the upper water column using a wide range of instrumentation, including a water sampler.

Deep-sea underwater vehicles are required to be large and heavy to withstand the pressures experienced at depth. This requires them to be deployed from large support vessels using cranes, making them unfeasible for the research presented in this thesis. Smaller AUVs which are designed for operation in shallow environments would be more suitable.

Developed by WHOI, the Remote Environmental Monitoring UnitS (REMUS) class of AUVs are one of the most commonly used AUVs in the world (Purcell et al. 2000). Of particular interest is the REMUS 100 model. This is a propeller driven, torpedo shaped vehicle that is generally 1.6 m long and weigh 30 kg (can change according to payload). They can operate at

depths of up to 100 metres. Their small, lightweight design makes them easily deployable by two operators from a small support vessel which allows them to be used as low cost, rapid response vehicles. Each year the REMUS AUVs play an integral part in numerous scientific and military applications. These include estuarine studies (Cruz et al. 1999), chemical plume tracing (Farrell, Li, Pang and Arrieta 2003) and for mine countermeasures (von Alt et al. 2001). The torpedo shape of this AUV is a common design choice. However this limits their ability to land on the seafloor without modifications to increase stability. An example of an AUV that may be suited to this application is the Morpheus AUV (Smith et al. 2001). This vehicle has a flat surface that could provide stability when landed. It features a high level of modularity allowing it to be adapted to suit a wide range of applications by adding sensors and other components. It has been deployed for mine counter measures in shallow waters. Another vehicle suited to this application is the Commonwealth Scientific and Industrial Research Organisation (CSIRO) developed Starbug class of AUVs. Starbug is described in detail in the next section.

2.5 Starbug AUV

This section describes the AUV platform that has been used for this research. This platform has been primarily developed by Dr. Matthew Dunbabin of the CSIRO ICT Centre, Autonomous Systems Laboratory (ASLab), and is known as Starbug (Dunbabin et al. 2005) (Figure 2.1). The motivation was to develop an AUV platform that was significantly cheaper than existing commercial products and which could be easily deployed from small boats or from the shore. This ease of deployment also means that the AUV can be operated with a minimal number of operators. This AUV is ideal for performing the XRF measurements because of a number of reasons. It has a twin hull design that would provide stability when landed, is small enough to be easily and cheaply deployed, and has a flexible hardware and software system that allows additional sensors to be added to its payload.

Figure 2.1: CSIRO's AUV called Starbug. It has various sensors on-board, including cameras, spectrometers, pressure sensors, an echo sounder and multiple GPS units (located in the tail). It has a mass of approximately 30kg depending on payload and is 1.2 m in length. Photo courtesy of the CSIRO ICT Centre.

2.5.1 Starbug Operations

Starbug is approximately 1.2 metres in length and weighs 30 kg. The buoyancy of the vehicle is manually controlled through the addition of weights and floats to the vehicle body. During missions with Starbug it is common practice to have it weighted so that it is positively buoyant (i.e. slightly floats). This allows easier communication with the vehicle while it is inactive, and also helps with recovery. When in the field a tether and visual aid in the form of a buoy are attached to the vehicle to assist with keeping track of its location, especially when submerged. Its design features two cylindrical hulls which are used to house various electronic components, as well as the batteries which power the vehicle. There are four 26 V lithium-ion batteries, each with a capacity of 12.6 Ah. This allows the vehicle to operate continuously for approximately 12 hours. The batteries can be recharged in the laboratory post-mission. A tail assembly contains additional electronics and sensors.

Computing power is provided by a VIA C7 processor running at 1.5 GHz with 1.0 GB of RAM. The processor is small, low powered and with efficient heat dissipation, making it ideal for use on a robotic platform. The vehicle

runs the Linux operating system, which along with the code base for the vehicle is stored on a compact flash card. Additional storage for log files and other data created during missions is provided by USB drives.

Penetrators in the hull provide ports which can serve multiple purposes. These ports differ in terms of what may be connected to them through different pin configurations. One port is used for a wired Ethernet connection, which is mainly used for communicating with the vehicle while it is in the laboratory. This port can also be used to supply auxiliary power to the vehicle via an external power supply to avoid draining the batteries. To power the vehicle on in the field a six-pin connector is placed in the power port, which is the same port used to charge the batteries. To enable sensors and other devices to be connected to the vehicle there are multiple serial and USB port connections available. These ports have receive and transmit pins, as well as both 12 V and 5 V power which can be supplied to external devices. Additional ports are used to connect to the thrusters.

Communication with the vehicle can be performed through the wired Ethernet connection. The AUV also has a Wi-Fi card, located in the tail, allowing wireless communication whilst in the field. Once submerged, communications are no longer possible. A Wi-Fi buoy has been developed that can facilitate communications, even while the vehicle is underwater (Breen and McCulloch 2012).

A total of five thrusters are used to propel the AUV around its environment. Two of these are rear thrusters, and are used for applying forwards or backwards thrust to the vehicle. They are also capable of controlling the heading through producing differential thrust. The remaining three are flat thrusters which are used to control the vehicle's roll and pitch.

2.5.2 Engineering Sensors

Starbug features a suite of engineering sensors to allow it to navigate about its environment and to provide information on its current state.

While on the surface of the water, Starbug navigates using three GPS units located in the tail USGlobalSat EM-408 (USGlobalSat 2012), San Jose

Navigation FV-M8 (San-Jose-Technology 2012) and LocoSys LS20031 (LocoSys 2012). An algorithm is used to combine the three GPS measurements to determine the vehicle's location. Once underwater, the GPS signal is attenuated, and the vehicle uses dead reckoning to track its location.

While submerged the AUV can determine its depth through the use of a pressure sensor, SSI Technologies PSI-100 (SSI-Technologies 2012). This needs to be calibrated in order to convert the raw pressure values to the appropriate depth. An echo sounder, Tritech PA500 (Tritech 2012), is used as an altimeter for measuring the height of the vehicle above the seafloor. This device is able to detect distances of between 30 m and 30 cm, with a nominal resolution of 1mm.

A digital compass measures the bearing of the vehicle, the Ocean Server OS5000-US (OceanServer 2012). A thorough calibration process is required for proper operation of the compass. This corrects for magnetic interference present in the vehicle which is known as hard iron effects. An Inertial Measurement Unit (IMU), the MicroStrain 3DM-GX1 (MicroStrain-Sensing-Systems 2012), measures the vehicle's roll and pitch.

For capturing images of its environment, Starbug is equipped with a downwards facing camera. Images are captured at a predetermined frequency for post-mission analysis. The images can also be used as input into computer vision algorithms to allow real-time, adaptive behaviour.

2.5.3 Scientific Sensors

The flexibility of the Starbug platform allows a variety of scientific sensors to be attached to measure a wide range of properties in the marine environment. A suitable method of attaching the sensors to the vehicle and appropriate drivers are required.

A multipurpose water analyser is a frequently used part of Starbug's scientific payload. This can measure the temperature, pH, dissolved oxygen content, turbidity and conductivity. A fluorometer is also frequently carried and is used to measure phytoplankton biomass and chlorophyll concentrations in the water. An optical emission spectrometer is attached to the

vehicle. This is used to measure the optical properties of the water column, and also the reflected light from the benthic habitat. This can be used for benthic species identification.

2.5.4 Applications

Starbug has been utilised in a wide range of applications. An image processing algorithm to identify the Northern Pacific Sea Star using shape recognition has been applied to images sourced by Starbug in the Derwent(Smith and Dunbabin 2007). It has been equipped with magnets to collect suspended particles from the water column. These particles were analysed in the laboratory using Mössbauer spectroscopy and identified elements that had both natural and industrial origins (de Souza et al. 2010). An optical emission spectrometer has been used to measure the light attenuation that occurs in the water column (Hartmann et al. 2009). Such a measurement is important in the application of autonomously identifying benthic habitat using hyperspectral images which is another potential application for Starbug (Davie et al. 2008).

2.6 Summary

This chapter has introduced the topic of AUVs. There are a number of existing platforms, however the majority are unsuited for the application discussed in this thesis due to their large size and impracticality. Smaller AUVs are designed for operation in shallow environments, such as estuaries. The CSIRO-developed Starbug provides a suitable platform for this research. It is able to be easily deployed by a minimal number of operators either from a support vessel or shore and its hardware and software components allow the easy integration of additional sensors. It features a twin hull design that provides a stable platform for landing on the seafloor.

Chapter 3

Automated XRF Analysis

3.1 Introduction

One of the major components in successfully increasing the scientific return of using autonomous machines to perform observations is the use of automated data analysis. This allows the software on-board the machines performing the observations to make sense of the data they are collecting in real-time, and use this information to perform their observations in a more intelligent manner. This on-board processing is necessary because it is often difficult or impossible to retrieve the data from the vehicle in real-time. Development of automated data analysis techniques provides the framework for future implementation of adaptive sampling approaches.

This chapter explores the use of automated data analysis for spectra produced from X-Ray Fluorescence (XRF) spectroscopy. Some key aspects of the XRF technique are provided. A more thorough discussion of the theoretical aspects is given in Appendix A. The problem of autonomously curve fitting spectra is then introduced, and an approach utilising genetic algorithms is developed. The experimental setup for laboratory analysis using the XRF system is described. This allows experimental spectra to be obtained in order to demonstrate the developed data analysis technique.

3.2 Background

3.2.1 X-Ray Fluorescence

The proliferation of portable XRF can be credited to two main technological developments (Fraser et al. 2008). These were the miniature X-ray tube for source excitation, and the non-cryogenic semiconductor detector for detection of X-rays. This meant that complete XRF systems could be provided in miniature portable packages that can operate at room temperature removing the need for complex cooling systems. Some basic background theory for XRF is described here (Beckhoff et al. 2006; Van Grieken and Markowicz 2001; and references therein). For a more detailed theoretical description see Appendix A.

When an X-ray strikes a material it can either be scattered or absorbed by the material's constituent atoms. In the absorption scenario, if the incident X-ray is of sufficient energy it can cause an electron to be emitted from the atom. This process is known as the photoelectric effect.

The ejected electrons can be from the inner shells (energy E_0) in the atom. This creates vacancies, resulting in the atom being in an excited state. In order to return to a stable state an electron belonging to a higher energy (energy E_j) shell drops down to fill the vacancy. When this occurs, the energy difference ($E_{tot} = E_j$ - E_i) between the two shells is emitted as a characteristic X-ray. Each element has a unique set of energy levels. Therefore the energy of the emitted characteristic X-ray is unique to the element that produced it.

Through detection and measurement of an X-ray's energy it is possible to identify the element that produced it. X-ray intensity increases with the concentration of a particular element within a sample. A typical XRF spectrum is constructed through counting the incidences of detecting an X-ray of a particular energy. Over time, peaks form within the spectra which are attributable to elements present in the sample. The area of these peaks is related to the concentration of the corresponding element. However there is not a straightforward relationship between the measured X-ray intensity and

the concentration of a particular element present in the sample. Consideration needs to be given to the output spectrum and the energy of the exciting X-rays, the efficiency of the detector, and the geometry of the source, sample and detector. Also relevant are the other elements present in the sample. The characteristic X-rays produced by an element in a sample could excite other elements present. This would result in some elements' concentrations being underestimated and others overestimated and is known as the matrix effect. For a full quantitative assessment these issues need to be corrected for.

One theoretical approach of converting the measured elemental peak intensities of a sample to concentrations is to use the fundamental parameters method which corrects for the matrix effects (Rousseau 2006; and references therein). This approach features two steps, calibration and analysis.

1. The *calibration* process involves quantifying instrument related factors using pure elements as calibration samples. This allows a theoretical intensity to be calculated for a sample of known composition.

2. In the *analysis* stage, an initial approximation is made of the sample's concentration based on the measured intensities. This approximation is used to calculate the theoretical intensity for a sample of that concentration. The difference in the measured and theoretical intensities is used to calculate a new approximation of the unknown sample's composition.

3. This process is continued in an iterative process until convergence is obtained between the measured and theoretical intensities.

To perform a full quantitative analysis using XRF spectroscopy these issues need to be corrected through sample preparation and extensive calibration. This is a difficult task in the context of the proposed technique, performing in situ measurements underwater. Therefore for the research presented in this thesis the XRF analysis will be of a semi-quantitative nature.

3.2.2 X-ray Detection

There are various techniques to detect the presence of X-rays, and determine the energy of those detected particles. The basic principle of an X-ray detector is to convert the energy of an incident X-ray into an electrical signal. This signal is then processed by electronics to arrive at the energy.

The main issues relating to X-ray detector performance are its efficiency and energy resolution.

1. The efficiency of a detector is what proportion of X-rays emitted are collected and absorbed. There are several limitations on the efficiency.
   (a) Geometrical efficiency. The active area of the detector, and its distance from the source of X-rays influences the amount of photons detected.
   (b) Intrinsic efficiency. This is the proportion of X-rays which enter the detector that actually interact with the detector material and are absorbed and is dependent on the mass attenuation coefficient of the detector material and the thickness of the detector material.
   (c) Photopeak efficiency. This is the fraction of photons which interact with the detector material, that deposit their full energy.
2. The energy resolution of an X-ray detector is how well the detector can distinguish between X-rays closely separated in energy. The spectral peak for X-rays of energy E_0 is broadened due to statistical fluctuations. The energy resolution is typically defined as the full-width-at-half-maximum (FWHM) of the measured peak.

There are several types of detectors that can be used for XRF spectroscopy (Knoll 2010). These include gas proportional counters, scintillation detectors and semiconductor detectors.

The most commonly used X-ray detectors for spectroscopy applications use semiconductors, which have the best energy resolution. The development of semiconductor detectors that can operate at non-cryogenic temperatures has had a large influence on portable XRF spectroscopy.

Semiconductors work through the production of charge carriers, known as electron-hole pairs, within their structure and are commonly made using either silicon or germanium (Floyd 1984). The charge carriers are created when an X-ray photon enters the semiconductor and ionises atoms within the material. When a voltage is applied across the semiconductor material the charge carriers flow towards the electrodes. The amount of electron-hole pairs collected at the electrodes of the semiconductor is proportional to the wavelength of the incident X-ray.

Further improvement can be gained through the use of Silicon Drift Detectors (SDDs) (Lechner et al. 1996). SDDs have concentric electrodes which cause the charge carriers to 'drift' to a collection electrode.

3.2.3 X-ray Sources

Initially, electrons were used as an excitation source. A hot filament would emit thermal electrons which would hit the target, creating the emission of characteristic X-rays. This form of excitation, however, led to some of the sample being altered due to heating, thus leading to changes in the composition. This led to the non-destructive excitation method of using X-rays being adopted for chemical analysis. To be suitable for use in a portable XRF system, a source needs to be low both in weight and power consumption.

One option is to use sealed radioactive excitation sources. These meet the criteria of being low weight and do not consume power. However, several disadvantages exist. A limited number of sources have suitable decay characteristics for XRF spectroscopy. Some commonly used examples include ^{55}Fe (suitable for elements between Na and Ti), ^{238}Pu (Ca - As), ^{109}Cd (Ca - Mo) and ^{241}Am (Fe - Gd). Due to the always on nature of the radioactive emission of these sources, there are safety issues regarding their use that may prove prohibitive. Special consideration needs to be given to shielding and interlock systems, even when the device is not in use.

A more commonly used source is the X-ray tube. These operate by a cathode emitting electrons which are accelerated towards an anode target. Upon striking the target, the electrons are decelerated and lose energy.

Through this process, a continuous spectrum of radiation is emitted, known as bremsstrahlung (German for braking radiation). Some electrons also cause ionisation within the target's atoms, causing emission of characteristic X-rays. Therefore, the emission spectrum from an X-ray tube features a broad bremsstrahlung spectrum as well as characteristic peaks from the target anode. Commonly used metals for the target include copper, molybdenum, magnesium, rhodium and silver. The type of anode may be chosen to optimise the excitation of elements of interest that will be analysed. Another selection issue is to avoid having the output spectrum of the X-ray tube increase the background component in the region of any important elements. The shape of the output spectrum may be changed through the use of filters. Filters, usually thin metal foils, are placed between the X-ray tube and the sample. These serve to reduce the background radiation around the region of interest. The tube voltage and current can be optimised to suit the particular application.

3.2.4 Outdoor Applications

XRF has been an extensively used technique in art and archaeology due to its non-destructive nature and convenience of field portable systems (Mantler and Schreiner 2000; Janssens et al. 2000; Shackley 2010). This enables researchers to assess what a particular artifact or artwork is made of and also aid in dating. Through analysing paintings it is possible to detect unknown pigments and increase understanding of traditional methods (Moioli and Seccaroni 2000). It is also possible to identify whether a particular painting is a forgery or not through the elemental analysis of the paint used. For example the presence of titanium in white paint spots indicates the presence of TiO_2 (Szokefalvi-Nagy et al. 2004). This was only used in painting from 1920, so its presence can provide evidence of a forgery or repainting. Analysis can also indicate whether or not an artifact is deteriorating due to environmental conditions such as pollution. An example of this is the analysis of Michelangelo's statue of David for determining the sulphur content, which is a catalyst for deterioration of stone monuments (Castellano et al. 2006).

One application area which has driven the development of robust miniaturised sensors, such as portable spectrometry systems, is interplanetary exploration. This arises through the unique requirements of the payloads for space science missions. These requirements include low weight, low power consumption and the ability to withstand the impact and stress of launching and landing.

The Viking landers on Mars each carried XRF spectrometers (III et al. 1973; Clark et al. 1982). The Mars rover, Sojourner, was equipped with an Alpha Proton X-ray Spectrometer (APXS) (Rieder et al. 1997). The Mars Exploration Rovers, Spirit and Opportunity, had an upgraded version of the APXS (Rieder et al. 2003). The Curiosity Rover, part of the Mars Scientific Laboratory payload, carries the CheMin (Chemical and Mineralogy) instrument. This can perform X-ray powder diffraction, which provides analysis of mineral structure, as well as XRF analysis (Sarrazin et al. 2005; Vaniman et al. 1998).

The benefit of a quick turnaround using field portable XRF systems is an attractive characteristic for environmental analysis. This allows rapid response to results of the analysis. Examples include the analysis of soils at hazardous waste sites to guide removal and rehabilitation programs and also the detection of lead in paints (Kalnicky and Singhvi 2001).

There have been previous studies into the use of field portable XRF spectrometers used to monitor heavy metal concentrations in marine sediment (Stallard et al. 1995). This study involved retrieving samples from the sea floor and analysing them both on a research vessel and in the laboratory using XRF spectroscopy. The results indicate that the wet samples analysed in the field were comparable to the dried, homogeneous samples analysed in the laboratory.

In the 1970s there was some work done on performing in situ measurements of marine sediments using XRF (Wogman et al. 1975; Wogman and Nielson 1980). The authors describe an experimental setup consisting of a ^{109}Cd excitation source and a cryogenically cooled solid state Si(Li) X-ray detector. A motorised scoop assembly allowed for sediment analysis to be conducted at different depths. The XRF device was tethered to either a

support vessel or a manned submersible. A cable between the device and support platform provided power, and is used for control and data transmission. An operator, either on the vessel or in the submersible, received data from the analysis in real-time. This provided the potential for decisions to be made on future analyses in the field.

3.2.5 Automated Curve Fitting of Spectral Data

An XRF spectrum consists of a combination of fluorescence peak emissions from a sample, each at a specific energy. The concentration of a given element is proportional to the number of counts under each characteristic peak present in the spectrum. Therefore any technique for evaluating the spectral data needs to be able to extract information from these peaks. The most straightforward approach is to interpolate the background component for each peak and sum the channel counts. However this does not take into account complexities such as overlapping peaks. Therefore the more commonly used technique is to approximate the acquired spectrum with an analytical spectrum. This requires a curve fitting process to extract spectral information.

There are two components in a spectrum that require curve fitting, the peaks associated with the elements present in the sample and the bremsstrahlung curve that originates from the X-ray tube. Elemental peaks within a spectrum have a Lorentzian distribution which can be described using three parameters: full width at half maxima (FWHM), peak position and intensity (Van Grieken and Markowicz 2001). Each Lorentzian function is of the form:

$$L(x, \Gamma) = \frac{\Gamma}{2\pi} \frac{1}{x^2 + (\frac{\Gamma}{2})^2} \tag{3.1}$$

where Γ is the full width at half maximum (FWHM), and x is the channel (or energy in keV).

A Gaussian peak provides an adequate approximation of the bremsstrahlung peak. This can also be described using three parameters, FWHM, peak position and intensity. The Gaussian function takes the form:

$$L(x, \sigma) = Ae^{\frac{(x-B)^2}{2\sigma^2}} \tag{3.2}$$

where σ is the FWHM, B is the peak position and A is the amplitude.

A curve fitting of an XRF spectrum consists of finding the best combination of these curves to match experimental data. The area under the peaks can be correlated with a semi-quantitative assessment of the elemental concentrations in the sample.

The values of the parameters characterising an XRF spectrum are typically determined with the help of the method of least squares, in which a curve is fitted to the measured points by the minimisation of the function:

$$\chi^2 = \frac{1}{n - n_p} \sum_{i=1}^{n} \frac{[N(e_i) - F(e_i)]^2}{F(e_i)} \tag{3.3}$$

where n is the number of measurement points, n_p is the number of parameters, the values of which are to be determined (including those associated with background), $N(e_i)$ is the measured spectral value at an energy point e_i and $F(e_i)$ is the sum of the values of Lorentzian functions at that point.

The value $F(e_i)$ of the function F at a given energy, is computed as a linear combination of Lorentzian functions:

$$F(e_i) = \sum_{k=1}^{n_s} I_k L(e_i - \delta_k, \Gamma) + B \tag{3.4}$$

Here n_s is the number of spectral lines, I_k represents the intensity of the line k, δ_k is the rotation of the line representing the middle point (i.e. the peak position) of the line and Γ_k is the width of the line k at half height. The symbol B stands for the function representing the bremsstrahlung radiation.

Software packages have been developed which perform this analysis in the laboratory. An example of this is a computer package called AXIL (Analysis of X-ray spectra by Iterative Least squares) (Vekemans et al. 1994). These software approaches need some level of user supervision to operate correctly making them unsuitable for automated analysis on-board robotic platforms. They also employ complex spectral approximations. For the purposes of the

application discussed here, real-time analysis on-board a robotic platform, an approach is needed that can be operated without human interaction. This leads to the investigation of an autonomous technique for the analysis of XRF spectral data.

An example of similar research is the automation of the analysis of Mössbauer spectroscopy (Salles et al. 1995; de Souza 1998; Ahonen et al. 1997; Klencsár 1997). Motivation for this work is the expediting of the analysis process and to reduce the reliance on experts within the field to analyse Mössbauer spectra. A combination of neural networks, fuzzy logic and genetic algorithms have (GAs) been used to analyse different aspects of the acquired spectra. Artificial neural networks have been used to correlate Mössbauer parameters that have been obtained through analysis with various structural properties of iron bearing minerals. The Mössbauer parameters are obtained by using GAs to curve fit the data. The results from the analysis using GAs are comparable to those obtained using commercially available fitting programs. Fuzzy logic is used to control the stopping condition of the GA based on expected relationships between Mössbauer parameters.

GAs have also been successfully applied to the analysis of XRF data (Brunetti and Golosio 2001; Brunetti 2013; Luo et al. 2006). The literature shows that using GAs can result in accurately fitted spectra. This includes the ability to resolve overlapped spectra. The reported benefits of GAs include their flexibility. The same software code can be easily adapted to suit a wide range of applications. Furthermore, resulting from their internal construction and operators, GAs are able to find the global minimum where local minima are frequent and are able to handle multidimensional data sets relatively easily. GAs are able to arrive at an approximate solution without supervision or user interaction. This approach fits well with automation needs, adding an interesting possibility to the applications of GAs in spectroscopic techniques for field robotics. A potential drawback of GAs is their slow convergence time. In the context of operating on-board a robotic platform this is not critical. The analysis can be performed concurrently while the platform performs other functions such as returning to the surface following a measurement. The convergence time for the application presented here is

in the order of one to two minutes, which does not impact on the operation of the robot.

3.2.6 Genetic Algorithms

Based on previous research that has been reported in the literature, GAs provide an attractive solution to fitting spectral data. Therefore an approach that utilises a GA will be implemented on-board a robotic platform to provide autonomous, real-time analysis of acquired XRF data. A general introduction to GAs is provided here.

The concept of using evolutionary algorithms to optimise systems began in the 1950s. GAs were invented by John Holland in the 1960s the University of Michigan (Holland 1975). Holland's initial goal was to study adaption in nature and ways in which it could be applied to computer systems.

A GA is an iterative algorithm which can be used to solve optimisation problems (Goldberg 1989). The basic premise is that several solutions (individuals) compete with each other for the opportunity of being selected to create new solutions (reproduction). The following outlines the main components of a basic genetic algorithm.

1. The algorithm starts with a randomly determined set of possible solutions, called the initial population or first generation. Traditionally the curve parameters of each initial solution are encoded as strings of binary digits (chromosomes).

2. Each individual in the population is assigned a fitness value. To assess the fitness of each solution in fitting the measured data, a fitness function is used. In our case we use the inverse value of the calculated χ^2 value (from Equation 3.1).

3. The next generation is created by pairwise exchanging bits in the binary representations of two parent solutions (crossover). A random crossover point is chosen. Parent solutions with higher fitness values are more likely to be selected for crossover. Thus, individuals with better fitness

are more likely to reproduce and pass on their characteristics to the next generation.

4. To introduce new genetic material into the population of solutions, some of the bits in each new solution may be switched randomly from zero to one or from one to zero. This is known as mutation. An example of this is shown in Figure 3.2.

5. The algorithm is usually stopped when the difference between the average fitness of the population and the best fitness encountered in the population is less than a pre-defined threshold. The average fitness grows closer to the best fitness over generations as the genetic operators tend to favour those chromosome structures for which the corresponding fitness values are large. The convergence of the algorithm can be improved through the use of elitism, in which the best individual in the old population replaces the worst in the new one.

An alternative to using a binary representation is to use real numbers for the chromosome. Crossover can occur through averaging the real values of the two parent chromosomes, and a Gaussian distributed value is used for mutation. The use of real values provides greater efficiency and accuracy over implementations using binary representation (Wright 1991).

The GA can be considered to be generic in the sense that it can be defined in a manner independent of the application. The only references to the application are made in the coding of the Lorentzian parameters of each X-ray peak to a chromosome representation and in the calculation of the χ^2 value of each solution.

3.3 The Implemented Algorithm

The software implementation of the GA was developed using the GAlib GA package, written by Matthew Wall at the Massachusetts Institute of Technology. The accumulated experimental spectrum is used as an input file. The parameters used to define the fitting are each represented by floating

point values with upper and lower bounds assigned. These parameters are the FWHM, intensity, and position of each elemental peak. Bounds for the FWHM are influenced by the energy resolution of the X-ray detector. The choice of bounds for the peak intensity is aided by an initial analysis of the experimental spectrum. This is calculated from the highest counts in the region of the expected peak. The peak positions are provided by a list of expected elements. This list contains the theoretical energies for each peak. The creation of this list can be aided by using available a priori information. This can include sediment samples analysed in the laboratory and results from previous studies conducted in the region. If there is no available information from the region being investigated, the spectral list would include all elements that would be of interest. The algorithm could include a peak search component. This would still require a spectral library to identify the peaks observed with their corresponding elements so as to facilitate any decision making on the collected results in real time. The floating point representations of each parameter value are then inserted into an array to form an individual's chromosome.

The implementation of the GA takes the following steps:

1. (Input) In addition to the file containing the measured absorption or backscattered values (i.e., the XRF spectrum), a spectral model is used at the start of the fitting routine. The spectral model consists of the possible position of expected elemental peaks (Deslattes et al. 2003).

2. (Background and bremsstrahlung curve) The background level needs to be evaluated from the spectrum. The background can also include the continuous bremsstrahlung spectrum which can be approximated using a Gaussian curve, whose parameters are added to the chromosome. This means that the entire solution is given by a background level, a Gaussian curve, and a series of Lorentzian peaks.

3. (Parameter bounds) The parameter bounds are determined on the basis of user-estimated peak positions from the spectral model, the maximum intensities around each peak position calculated from an initial analysis

of the experimental spectrum, the spectral resolution of the instrument and the computed background level.

4. (Initial population) An initial set of solutions is created by the random generation of values representing the curve parameters within the specified bounds.

5. (Fitness calculation) The fitness of each solution is calculated as the inverse value of χ^2 computed on the basis of the measured spectrum and the linear combination of Lorentzian functions and a background component corresponding to the parameter values extracted from the binary string. The sum and average of all fitness values are computed (eq. 3.3).

6. (Reproduction, crossover and mutation) The probability of an individual being selected for reproduction is proportional to its percentage contribution to the overall fitness. A roulette-wheel-style selection process is used with sectors allocated to individuals in proportion to their fitness. Two parent solutions are chosen and their curve parameters combined to produce two child solutions. This is demonstrated in an example shown in Figure 3.1.

   Each curve parameter has a probability to be mutated. This occurs by adding a Gaussian distributed value to the selected parameter to introduce new genetic material to the algorithm. This is shown in Figure 3.2.

7. (Elitism or cloning) To ensure genetic material of high fitness is preserved the worst solution in the new population is replaced by the best solution of the previous generation. This is also important to keep the best results so far registered.

8. (Iterate through generations until stopping condition is achieved)

9. (Stopping) The algorithm is subject to dynamic stopping conditions which are tailored to the need of a quick spectral assessment for guiding an adaptive sampling strategy. The coefficient of variance of each

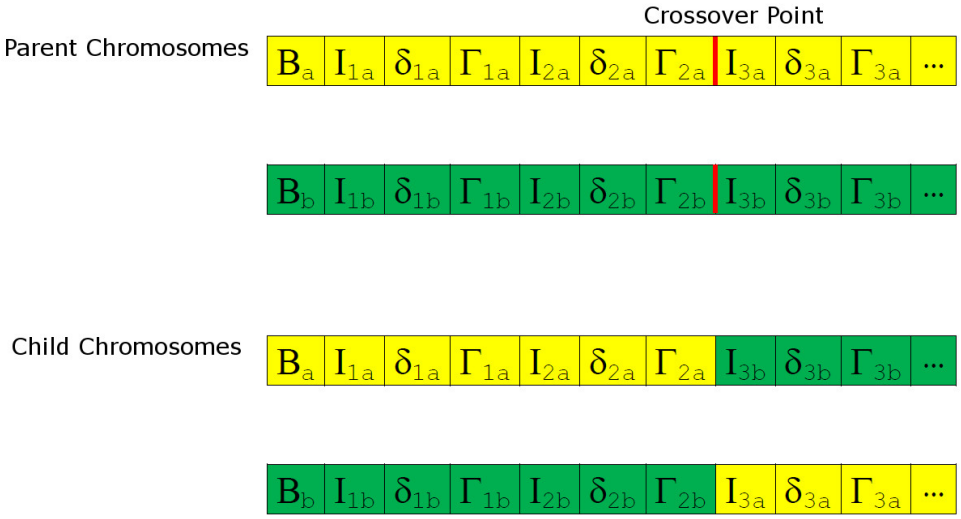

Figure 3.1: Example of crossover involving two parent solutions, made up of peak parameters, to create children.

parameter is used to indicate the rate of change of each component of the solution. When the coefficient of variance of the parameters of one peak become small enough to indicate further generations would provide negligible improvement, the parameters for that curve become fixed and do not change with further generations. The algorithm runs until each peak's parameters have stopped changing.

10. (Final output) The algorithm computes the final peak intensity and area on the basis of the extracted parameter values corresponding to the best solution.

The output from this algorithm is used to provide a semi-quantitative assessment of the concentrations of metals of interest. To perform a full quantitative study of the concentrations present is a complicated process and is beyond the scope of this thesis. Performing in-situ measurements of this nature in environments such as underwater it is difficult to accurately model

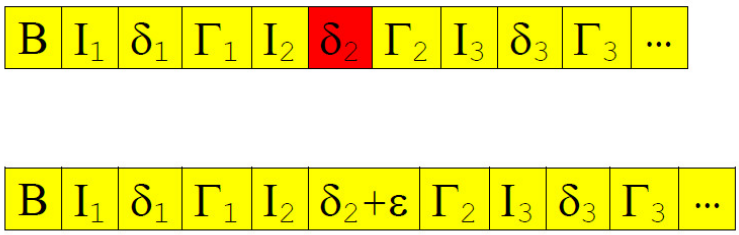

Figure 3.2: Example of mutation of a curve parameter by adding a small value, ϵ, to its value.

the various variables associated with the measurement scenario. These include the geometry of the sensor relative to the sediment being analysed, the grain size of the sample and the moisture content. Correcting for the aforementioned matrix effects would also require extensive calibration. Therefore the results presented throughout this thesis are of a semi-quantitative nature. This is achieved through the use of relative concentrations for each measurement using the Relative Spectral Area (RSA) of each element. This is calculated using the following equation:

$$RSA_x = \frac{A_x}{A_{tot}} \tag{3.5}$$

where RSA_x is the relative spectral area for an element of interest, x, A_x is the area under the spectral peaks associated with x, and A_{tot} is the total area contained under all peaks of the spectrum.

This algorithm requires several parameters relating to the GA to be determined beforehand. These are the initial population size, mutation and crossover rate, and the criteria for the stopping condition. The values for these parameters are determined through a trial and error process. This involves balancing the accuracy of the fitting with its efficiency. This criteria involves the number of generations the coefficient of variance of each parameter is calculated over and a suitable threshold the resulting value is compared

against.

3.4 The XRF System

In order to present results of the developed automated data analysis technique it is necessary to describe the experimental setup that will be used in the laboratory. This includes the components of the XRF system, the X-ray tube and detector.

3.4.1 X-Ray Tube

To provide the excitation needed for XRF an X-ray tube is used. The tube, supplied by the company Amptek (Amptek 2012), is known as the Mini-X (Figure 3.3).

Figure 3.3: Amptek's X-ray tube, the Mini-X. The main aluminium body is 14.8 cm x 5.8 cm x 2.5 cm.

It uses a 1.5 μm thick tungsten target to produce X-rays. Tube voltage is between 10 and 40 kV, while the current is between 5 and 200 μA. Communication with the device is done via a USB connection.

The device is air cooled, and cannot be operated in an ambient temperature of greater than 50 °C. The Mini-X has a beryllium end window. The approximate dose rate of the device is 800 μGy/s operating at maximum voltage (40 kv) with a current of 50 μA at a distance of 30 cm. X-rays are emitted from the tube in a 120 ° cone. If a more concentrated beam is required, a brass collimator with an aluminium insert can be screwed into the Mini-X. The collimator has a 2 mm diameter hole. The device has several safety controls and indicators. A flashing LED on the rear of the device and a beeper indicates when X-rays are being produced. To prevent accidental emission of X-rays the Mini-X features a hardware interlock system. For X-rays to be produced, the interlock needs to be enabled through connecting the two terminals, shorting the interlock. When the interlock is disabled during X-ray production the device resets, ceasing production of X-rays. Since it resets, re-enabling the interlock will not result in the resumption of X-ray production.

3.4.1.1 Filters

A set of filters are supplied with the device. These filters are used to modify the output spectrum of the X-ray tube so it better suits a particular application. The filters included are aluminium in two thicknesses, 1016 μm and 254 μm and copper, molybdenum and silver all in 25.4 μm. These filters are screwed on with the collimator, except for the 1016 μm aluminium filter which is held in place with a special cap over the end of the collimator.

Determining the correct filter to use, if any, is an important step in preparing the system to perform measurements. If the output spectrum overlaps with important element peaks, then the intensity of those peaks may be overestimated. Therefore a filter that removes the unwanted output spectrum in the energy range where observed peaks from a sample are expected is desirable.

The heavy metals that will be studied predominately have peaks in approximately the 8 to 13 keV range. The unfiltered output spectrum overlaps significantly with this range. Through the use of the supplied filters,

it is possible to remove some of the unwanted spectrum. Figure 3.4 show a comparison between using no filter and with the 1016 μm aluminium filter in place. It successfully filters out the majority of the peaks associated with the tungsten target. The large peak present in the spectrum is due to bremsstrahlung radiation, and can be accounted for during data analysis.

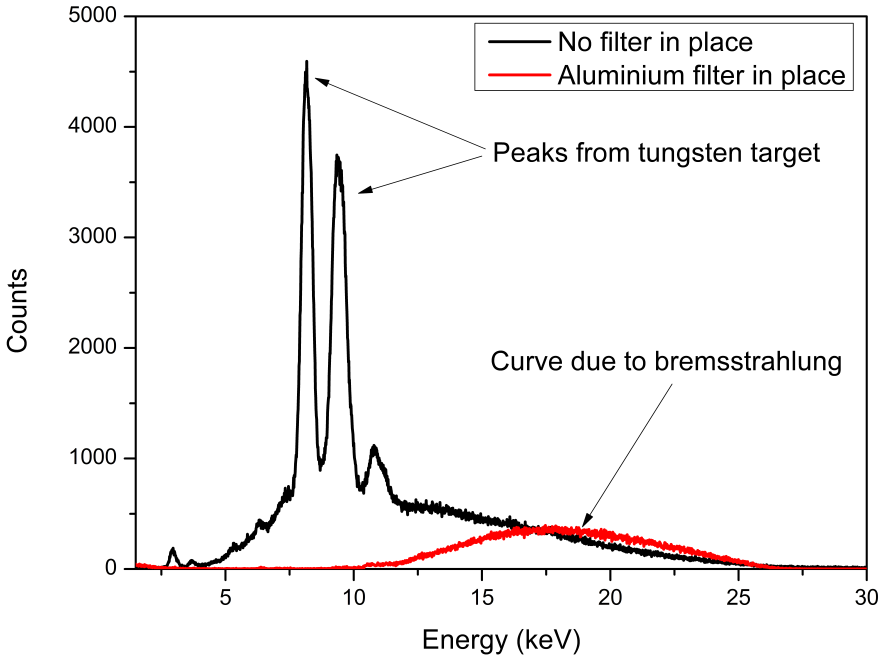

Figure 3.4: A comparison of the X-ray tube's output spectra without a filter in place and with the Al filter fitted.

3.4.2 X-Ray Detector

The X-ray detector to be used for this work is the X-123 model, also supplied by Amptek, and is shown in Figure 3.5. The X-123 is a complete X-ray detection system. It combines the X-ray detector (XR-100CR), preamplifier, digital pulse processor and multichannel analyser (DP4), as well as the power supply in one unit.

The XR-100CR uses a Si-PIN detector that was included as part of the scientific payload on the Mars Pathfinder mission as a sensor on the Sojourner rover (Rieder et al. 1997). The area of the detector is 25 mm^2 and has a thickness of 500 μm. It uses a thermoelectric cooler to reduce electronic noise. This removes the need for liquid cooling, allowing room-temperature operation.

The digital pulse processor takes the output from the preamplifier and digitises it. Some digital processing steps are applied to the signal, and the peak amplitudes are detected. These amplitudes are then stored in bins, or channels, creating the energy spectrum. This spectrum can then be transmitted over the DP4's interface to a computer for further analysis.

Figure 3.5: Amptek's X-ray detector, the X-123. Its dimensions are 7 cm x 10 cm x 2.5 cm.

The dimensions of the device are 7 cm x 10 cm x 2.5 cm, with the detector mounted on an extender which protrudes 5.5 cm out from the unit's body. A 1 mm thin beryllium window protects the detector and due to its low attenuation still allows the passage of low energy X-rays. It weighs 180 g, which combined with its compact size, make it ideal for use on a robotic platform. The unit requires an input voltage of approximately +5 V_{DC}, at a

current of 250 mA. Communications are handled via either a USB connection, or serial RS232.

The system has a guaranteed energy resolution of between 190 and 225 eV FWHM at 5.9 keV. It has a maximum count rate of up to 2 x 10^5 counts per second. The system can detect characteristic X-rays of energy between 1 and 25 keV with an efficiency of greater than 25 %. X-rays can still be detected outside this range, albeit with reduced efficiency.

3.4.2.1 Calibration

The X-ray spectrometer measures counts in channels. To convert these channels to an energy value, calibration needs to occur. This involves obtaining spectra of materials containing known elements. The resultant spectrum will then contain known peaks. The peaks are identified with their corresponding energies to produce a calibration equation which relates channel to energy value. The supplied software performs this calibration. Several materials that would result in easily identifiable peaks were used for calibration purposes. These were lead, an Australian 50 cent coin, which contains copper and nickel, and sterling silver. An example of the peaks generated for the sterling silver sample is shown in Figure 3.6.

Some peaks are not clearly defined, or overlap with neighbouring peaks, making them unsuitable for use in calibration. The data used for calibration is shown in Table 3.1.

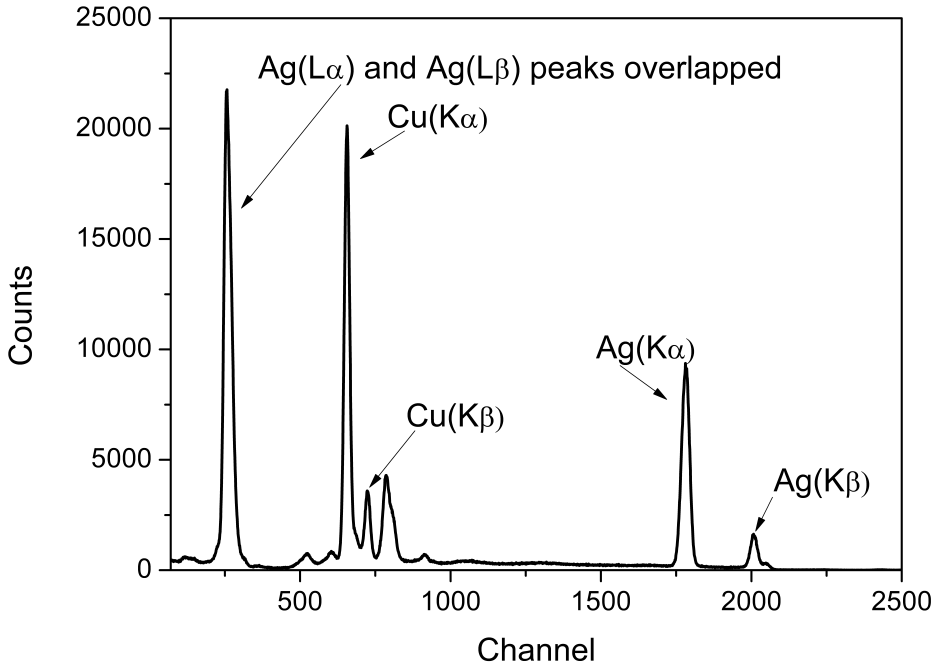

Figure 3.6: Spectrum of silver used for calibration purposes. Peaks used for calibration are labelled.

Figure 3.7 shows the relationship between this data.

This data has been fitted with a linear equation with high accuracy (R^2=0.99) to arrive at the calibration equation (Eq. 3.5).

$$energy = 0.0125 \times channel - 0.142 \tag{3.6}$$

Note that changing the gain value for the X-ray detector will require a recalibration.

3.4.3 Experimental Laboratory Setup

In order to evaluate the curve fitting algorithm, experimental spectra need to be obtained in a laboratory setting. When performing measurements with the XRF system there needs to be sufficient shielding protecting the operator

Material	Element	Peak	Observed Channel	Theoretical Energy eV
Lead	Lead	L_α	856	10551.20
Lead	Lead	L_β	1021	12613.00
Coin	Nickel	K_α	608	7477.72
Coin	Copper	K_β	722	8906.90
Silver	Copper	K_α	656	8048.11
Silver	Silver	K_α	1781	22162.99
Silver	Silver	K_β	2007	24943.10

Table 3.1: Known peaks identified from calibration samples and their theoretical energies.

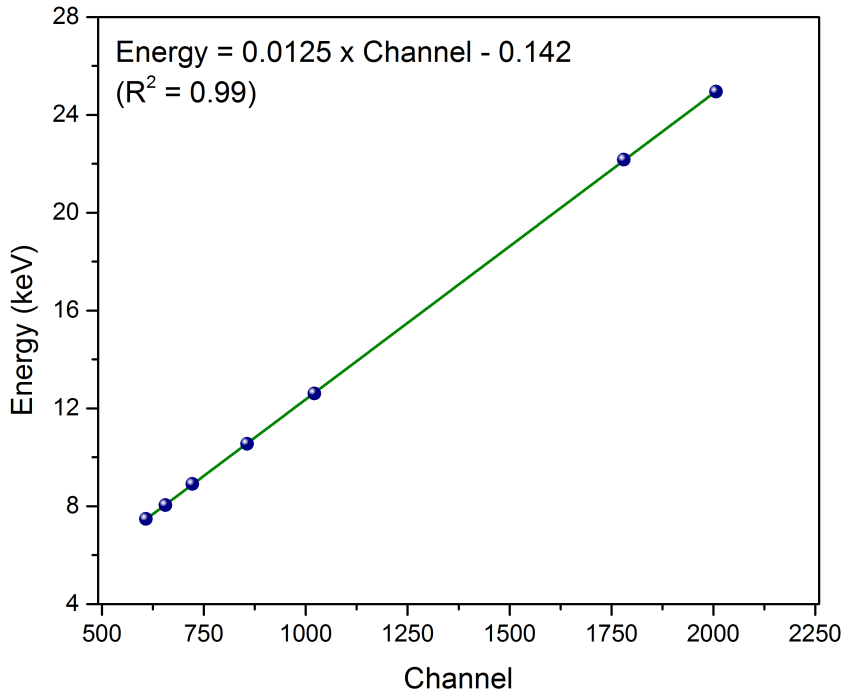

Figure 3.7: The calibration data showing the relationship between observed channel and energy. This data has been fitted with high accuracy.

from potentially harmful radiation emitted by the X-ray tube. To this end,

a household safe was used to house the XRF system during measurements. This also serves as a secure location to store the equipment. The safe is constructed from 6 mm thick steel and has internal dimensions of 598 mm x 408 mm x 360 mm. It has four 16 mm bolt holes in the base, through which cables that are used to supply power and communications can be fed. These holes can also potentially provide a path for X-rays to escape and to alleviate this a lead floor was installed. This floor was designed using lead partitions attached to its underside in such a way that any X-rays that do reach the bolt holes have to undergo multiple reflections resulting in them being attenuated to safe energies. The safe was tested with a Geiger counter while the X-ray tube was producing X-rays and the radiation levels were no higher than background. To help hold the X-ray detector and X-ray tube in position while analysing a sample, a retort stand is used. Figure 3.8 shows the experimental setup in the laboratory.

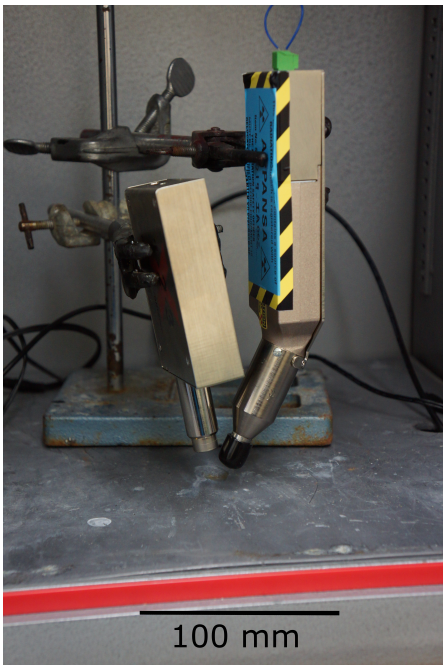

Figure 3.8: The X-123 and Mini-X in the safe, held in position by a retort stand for laboratory analysis.

For the successful operation of the XRF system in the field a portable

housing is required. It is this field deployment that represents the original contribution involving the described XRF system. This will feature an end-cap which is specially designed to hold the X-ray detector and emitter securely in place. Measurements performed in the laboratory will use this end-cap to replicate conditions that will be experienced underwater. It features a thin window through which X-rays pass, the design of which is important to the overall performance of the system. The material used must have low attenuation of X-rays. It must also be thick and strong enough to maintain its waterproof qualities at depth and to deal with the stresses associated with landing on the seafloor. The seafloor can potentially be abrasive and there is the risk of damage to the cap through impact while landing.

Based on these considerations, the thickness of the window and the material from which it is made are important design decisions and represent an original research component. The work presented in (Wogman et al. 1975; Wogman and Nielson 1980) use a beryllium window. Beryllium has very low X-ray attenuation (Hubbell and Seltzer 1995). However, it is a brittle material and has some toxicity, making it problematic to work with. Therefore it has not been considered for use in the work presented in this thesis. A material consisting of carbon, which also has a low attenuation coefficient, potentially represents a viable option for the end-cap material. A plastic known commercially as Delrin, which is a polyoxymethylene homopolymer with a chemical formula of CH_2O, was used to construct a prototype. Delrin is a strong material with high abrasion resistance. Tests of the level of attenuation using a 50 c Australian coin as a target were conducted using 3 mm of Delrin compared with no material present. This showed that Delrin resulted in a significant reduction in counts detected and also attenuation of peaks associated with the sample. The only peaks present are attributable to the output spectrum of the X-ray tube, both the tungsten peaks and the continuous bremsstrahlung radiation. This indicates that Delrin attenuates the X-rays to such an extent that it is unfeasible as the end-cap material. An alternative is high density polyethylene (HDPE) the chemical formula of which is C_2H_4. The oxygen atom in Delrin has the largest attenuation coefficient of the elemental constituents. This may suggest that HDPE, with

only carbon and hydrogen atoms, will have lower attenuation. Attenuation is still higher than with no material present, but the expected elemental peaks are clearly visible. The number of counts is also significantly higher than the Delrin. Therefore the end-cap has been designed with a 3 mm window made of HDPE. The attenuation of Delrin and HDPE compared to no material present is shown in Figure 3.9.

The housing has been successfully tested in a pressure chamber to a depth of 100 m.

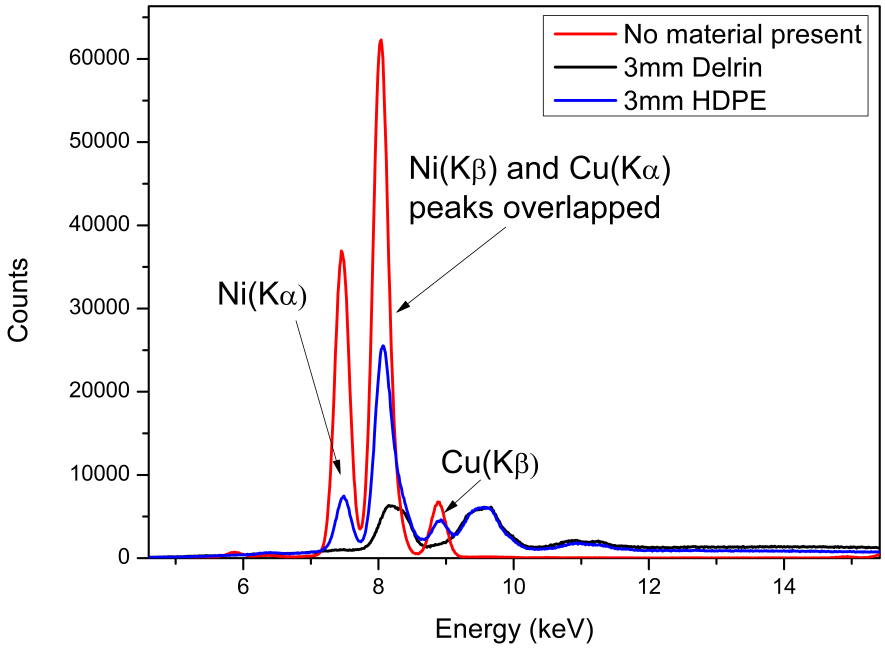

Figure 3.9: Comparison of the spectra obtained of a 50 cent coin target with X-rays being transmitted through Delrin and HDPE. Also shown is the spectrum with no material present.

3.5 Results and Discussion

The technique of performing automated data analysis has been demonstrated on some sample spectra that have been acquired in the laboratory. The GA had a population size of 200 individuals. Each pair of individuals selected for reproduction has a 90% chance of producing new individuals. New genetic material is introduced through having a mutation rate of 5%. The algorithm stops iterating when the curve parameters of the fittest individual have had negligible variance over 20 generations. The algorithm outputs the percentage contribution of each identified peak to the whole spectral area (WSA) of the spectrum.

Figure 3.10 shows a spectrum of stainless steel that has been obtained under ideal laboratory conditions with no background component present. This spectrum has undergone curve fitting. Dominant lines are associated with concentrations of iron, chromium and nickel, with minor contributions of molybdenum and copper. These elements, and relative concentrations detected are indicative of stainless steel.

The remaining spectral examples have resulted from conditions that more closely resemble those that will be present during the taking of in situ measurements underwater. This is achieved by seating the XRF system in the HDPE housing to show the effects of attenuation. Table 3.2 shows the expected elements that form the spectral list used as input for the GA.

Figure 3.11 shows a spectrum from a cast iron target. As to be expected, the data analysis algorithm identifies the sample being almost entirely iron.

The other spectrum presented here is an actual sediment sample that has been analysed in the laboratory. This was a wet sample that had not undergone any preparation (Figure 3.12). Iron is the dominant element present in this sample, followed by strontium. Strontium is most likely present as a constituent of the seawater. and its high relative concentration may be caused to some degree by the matrix effects.

An alternate metric to the relevant spectral area is looking at the ratios of elements present. To remove the influence of the other elements (Br and Sr) a ratio of the heavy metals (Zn and Pb) to Fe can be used. The following

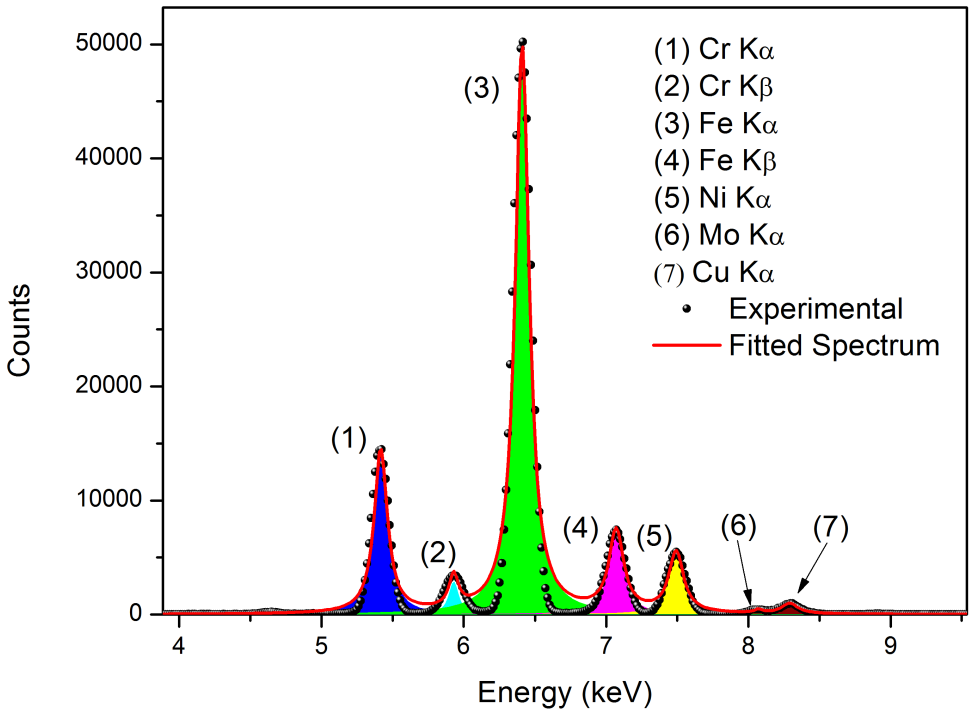

Figure 3.10: Experimental and fitted spectrum for a stainless steel sample. The percentage contribution to the total spectral area was 17.6% WSA chromium, 69.1% WSA iron, 10.8% WSA nickel, 1.0% WSA molybdenum and 1.5% WSA copper. There are some areas evident that show fitting errors, especially at the tails of peak 3. (Breen et al. 2011)

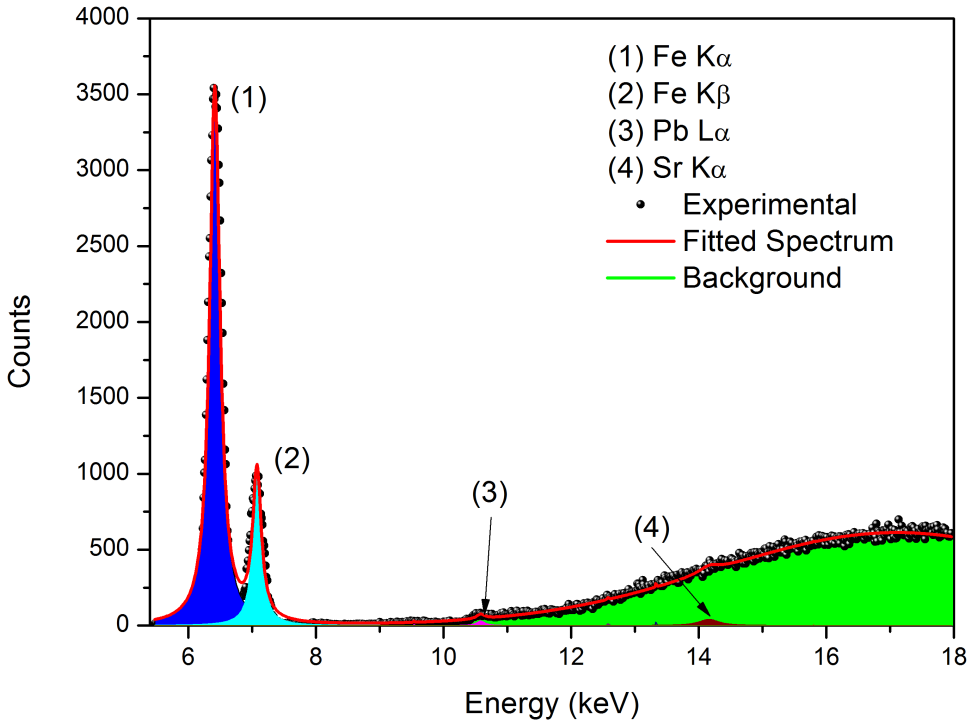

Figure 3.11: Experimental and fitted spectrum for a cast iron sample. The percentage contribution to the total spectral area was 97.6% WSA iron, 1.8% WSA strontium and 0.6% WSA lead.

Element	**Peak Type**	**Energy keV**
Iron	Kα	6.40
Iron	Kβ	7.06
Zinc	Kα	8.64
Zinc	Kβ	9.57
Lead	Lα	10.55
Lead	Lβ	12.61
Bromine	Kα	11.92
Bromine	Kβ	13.29
Strontium	Kα	14.16
Strontium	Kβ	15.83

Table 3.2: List of expected elements used for setting initial parameter bounds.

equation shows the calculation to determine the relevant ratio.

$$fracspectralarea(Zn + Pb)spectralarea(Fe) \tag{3.7}$$

For this sample the ratio would be 0.13, indicating that there is more than seven times the relative spectral area of iron than the heavy metals.

The fitted spectra generally show good agreement between fitted curves and the experimental data. However some miss-fits are evident from these spectra, especially in the vicinity of the peak tails. The fitted peaks have wider tails than the experimental data and may be due to instrument effects. This may be corrected through the use of a different type of peak. A Voigt peak, which is a combination of a Lorentzian and Gaussian line, may be used. However this will require a significant increase in the number of GA parameters used to represent the experimental spectrum. Parameters from both a Lorentzian and Gaussian line for each expected peak need to be added, as well as a factor representing the proportion contribution of each peak to the final fitted solution. These extra parameters would increase the complexity of the implemented algorithm and time taken to converge to a solution. For the purpose of performing semi-quantitative analysis in real-time on-board an AUV the fittings achieved are satisfactory.

The relative concentrations of the elements are given as the percentage

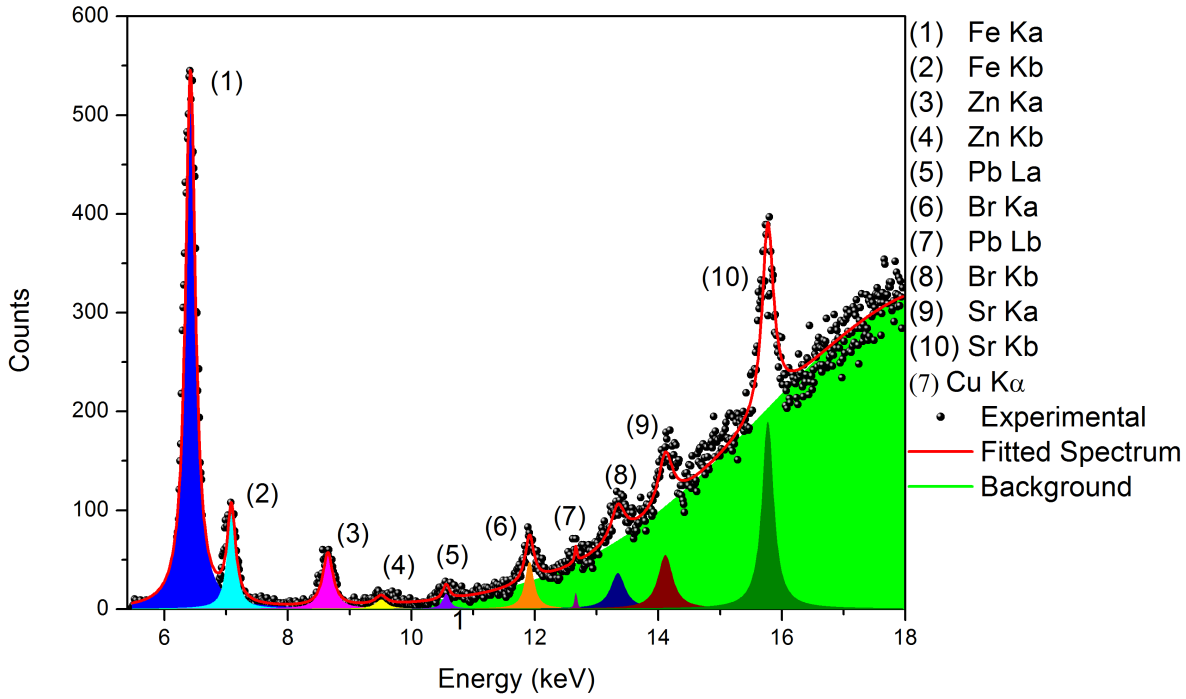

Figure 3.12: Experimental and fitted spectrum for a wet sediment sample. The percentage contribution to the total spectral area was 57.0% WSA iron, 6.0% WSA zinc, 8.7% WSA bromine, 1.3% WSA lead and 27.0% WSA strontium.

contribution of each element detected to the overall spectral area. These results are semi-quantitative and give an indication of the relative abundance of each metal. This information is sufficient for the AUV to make autonomous decisions on measurement strategy.

Tests have shown that the algorithm takes several minutes to converge to a solution when run on the AUVs computer. The algorithm can be run concurrently with the AUV performing other tasks, such as moving between measurement locations or resurfacing after doing an analysis. The times taken would not adversely affect operation of the AUV and it would be feasible to run the algorithm in real-time. Should a trade-off between accuracy and execution time be needed, the algorithm is flexible enough to allow such adjustments. This could be done through changing population sizes, the stopping condition, parameter intervals and several other customisable options.

3.6 Summary

This chapter has discussed several aspects of the field of XRF spectroscopy. The technique offers a non-destructive method to detect multiple elements within a sample, and due to technological advancements it is possible to have an entire XRF system in a field-portable configuration. The most common of these consists of a semiconductor X-ray detector and a miniature X-ray tube. This enables it to be utilised in a wide range of applications, such as in the field of art and archaeology as well as for environmental analysis. One area that has been discussed in the literature in which the technique has been used is the analysis of marine sediments. Examples of previous studies that have been reported include the analysis of retrieved samples on-board a ship using a portable system, and also the in situ measurement of sediments.

An important component of this technique is the analysis of XRF spectra to obtain information on the elemental constitution of a sample. This chapter has described a curve fitting approach using GAs to perform an automated analysis of acquired XRF spectra. This allows the unsupervised analysis of collected data on-board an AUV to facilitate decision making in

real-time. The algorithm calculates the peak area associated with each element and correlates this with a semi-quantitative assessment of elemental concentration. This work has provided a foundation for future development in adaptive sampling techniques

The XRF system and experimental setup for experimental analysis has been described. One component of the housing for the system that is to be attached to the AUV was discussed. This was an end-cap, through which X-rays pass, that is to be placed in contact with the sediment to be analysed. The choice of material for this end-cap is important as it must be tough enough to handle contact with the seabed as well as have low attenuation of X-rays. A materials investigation found that HDPE was a suitable choice.

Chapter 4

Control of an AUV

4.1 Introduction

AUV behaviour refers to how they interact with their environment. This includes how they navigate and sense underwater. AUVs exhibit the necessary behaviours through executing individual tasks on their on-board computer. These use sensed information on the current environment and state of the vehicle to perform specific actions. These actions can include activating the thrusters to change the vehicle's location or orientation, or triggering the commencement of environmental sensing using scientific instruments. A simulated environment can be used as a test bed to aid development.

This chapter explores the development of the behaviours that will allow the AUV to successfully perform the XRF measurements that are the focal point of this research. The key behaviours required are the landing of the AUV on the seafloor and the process of performing the measurement. Also investigated is the integration of the XRF system with the AUV.

4.2 Simulated AUV Environment

The development cycle required for programming a robotic platform, such as an AUV, is potentially time-consuming. Testing of behaviours and other code require field missions to observe and evaluate performance. Debugging of

any issues then requires returning to the laboratory for further development. While the vehicle is underwater it cannot be directly observed. Post-mission analysis of the sensor data is then required to determine if the vehicle behaved correctly. To help alleviate the cumbersome process of testing and debugging on the platform, a simulated environment has been used. This is an extension of work done by the CSIRO's QCAT. The simulator has been developed using the Open Robotics Automation Virtual Environment (OpenRAVE) (Diankov 2010). This provides integration of the Starbug code base with a three dimensional graphics interface. The simulation uses a three dimensional model representation of the AUV and the environment, including the seafloor. This is shown in Figure 4.1.

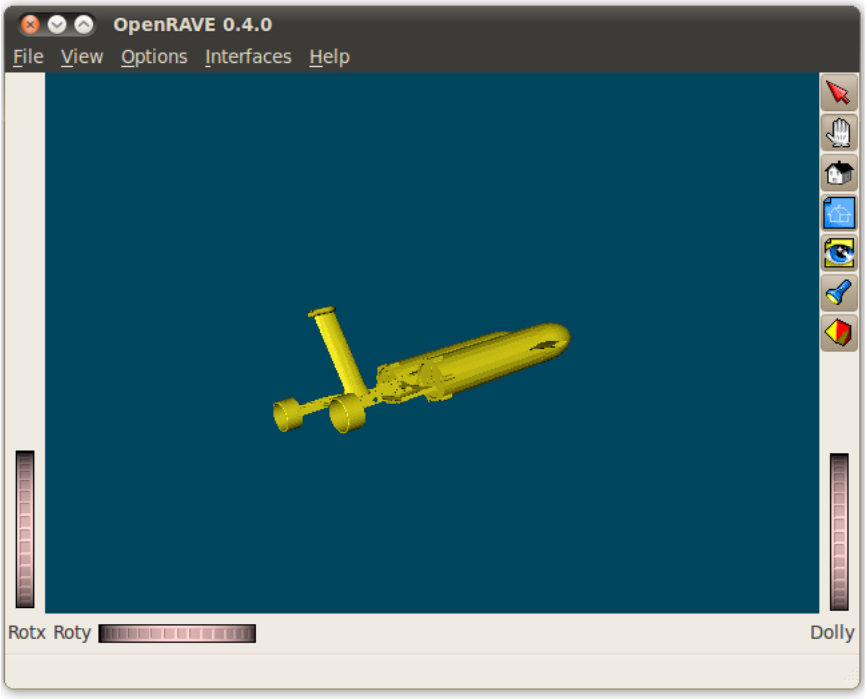

Figure 4.1: Screenshot example of the Starbug model exploring a simulated environment in OpenRAVE.

The location and orientation of the vehicle relative to its environment is returned by the simulator which is then used to replicate engineering sensor output. Starbug's thrusters are also modelled within the simulator and allow

the vehicle to move throughout the environment. Starbug tasks are run in the same manner as in the field and allow the vehicle to interact with the simulated environment. The performance of the programmed task can be evaluated through observing the vehicle's behaviour as it executes the code. This has proven to be a valuable tool for learning the Starbug code environment, and developing, testing and debugging relevant behaviours to provide the best chance of success when the vehicle is deployed in the field.

4.3 Landing

An important part of performing an XRF measurement is the controlled descent and landing of the AUV on the seafloor. For a measurement to be successfully performed, the vehicle needs to land on the seabed in such a manner that the XRF housing has sufficient contact with the sediment and remain stationary for the duration of the measurement to enable spectra of high quality to be collected. This section discusses the work that has been undertaken to successfully land the AUV and highlights the challenges that were encountered and overcome.

4.3.1 Previous Work

There has been some work done on landing of AUVs. There are various motivations for the development of a vehicle with landing capabilities. To conserve the limited power available to an AUV it is sometimes advantageous to sit on the sea floor for extended periods of time and perform long-term measurement tasks. Some measurement tasks require close proximity to the sea floor. These applications can include microscopic analysis of aspects of the sea floor. One important aspect of landing is how to control the vehicle's descent.

The buoyancy of vehicles can be controlled in some instances. This can be done using tanks which can be filled with water through the activation of valves when required to make the vehicle descend (Liu et al. 2011; Wang et al. 2007). These tanks also provide stability whilst landed. Ballast weights

are discarded from the vehicle to allow it to ascend to the surface.

Another approach is to have a negatively buoyant vehicle which can sink to the sea floor (Sangekar et al. 2010; 2011). A wing structure is used to compensate for the negative buoyancy when in forward motion and landing struts are used for added stability. The work presented in these papers also describes the use of a laser profiling system to identify areas of the sea floor that are flat enough on which to land safely.

In the literature thrusters are not used for landing through making the vehicle negatively buoyant by using a variable buoyancy system or weights. Thrusters can disturb the material present on the sea floor, which may be disadvantageous in some circumstances, or introduce vibrations which may interfere with sensors during measurements. Power consumption will also be minimised due to the thrusters not being operated.

4.3.2 Landing with Starbug

Starbug does not have any automatic mechanism to adaptively change its buoyancy, such as ballast systems or pumps. This means that it needs to be weighted according to the required buoyancy at the start of every mission. For deployment on normal monitoring missions, Starbug is weighted so it is positively buoyant. This makes communication and recovery of the vehicle easier due to it floating while not currently on a mission.

An initial attempt at landing the AUV was made while it was positively buoyant. This required the use of the thrusters to push the vehicle down and keep it in position for the duration of the measurement. Tests indicated it successfully reached the bottom, but appeared unable to maintain its position. This may indicate that the thrusters are not sufficient to keep the vehicle on the sea floor for any extended period of time. Visual inspection of the thrusters post mission showed fouling caused by contaminants from the sea floor. This included seaweed and other material that were being sucked into the thrusters. Shrouds were installed over the thrusters to prevent fouling, though these would not be effective with fine particles that may be disturbed from the sediment. These particles could impede the thrusters'

performance. Additionally, disturbance of the sediment layer by the operating thrusters is not ideal from a measurement point-of-view. Having the thrusters continually operating throughout the measurement process is also a power consumption issue. These issues suggest that the vehicle may have to be made negatively buoyant in order to land successfully, as is supported by the related work found in the literature.

Starbug was made negatively buoyant through the addition of weights. The weights were distributed about the vehicle such that the centre of mass was as close to the location of the XRF housing as possible. A support was added to the front of the vehicle to improve the vehicle's stability while sitting on the seafloor.

The landing procedure is controlled by a programmed task. The vehicle descends at a constant rate while maintaining a pitch and roll of zero degrees. When the altimeter senses the seabed at a pre-determined distance below the vehicle, approximately 0.5 m, the thrusters are all disengaged and the AUV allowed to free-fall the remaining short distance. The AUV control software needs to be able to identify when the vehicle has finished its landing procedure and has settled on the seafloor. This is achieved by using the vehicle's pressure sensor to measure the present depth. When the standard deviation of the measured values for depth remains steady for a period of time, then the vehicle can be identified as having landed. Algorithm 4.1 outlines the code controlling this landing behaviour.

Algorithm 4.1 AUV Landing Procedure

```
Commence descent to seafloor
while (Vehicle is greater than 0.5 metres above seafloor) do
    Maintain roll and pitch of zero degrees
end while
Turn off thrusters
while Depth values from pressure sensor have large standard deviation
over a given period of time do
    Continue free-fall descent
end while
Identify vehicle has landed, proceed to performing measurement
```

Evaluation of a landing attempt can be made using the engineering data collected by the sensors on-board the vehicle. The relevant data is the standard deviation of the vehicle's depth, pitch, roll and yaw for the duration of the landing. Analysis of this data can indicate whether the vehicle was stationary while it was situated on the seabed. For comparative purposes the sensor readings from the vehicle while it is stationary in the laboratory are used and are shown in Figure 4.2.

The standard deviation of the recorded values for depth, pitch, roll and yaw for a five minute period while the vehicle was stationary in the laboratory are 1. cm, 3 mrad, 2 mrad and 3 mrad radians respectively. Figure 4.3 shows the same data from a landing attempt in the field.

The standard deviations for the vehicle during the period it was landed on the seabed are 5.5 cm for depth, and 3 mrad, 10 mrad and 5 mrad for pitch, roll and yaw respectively. These values are similar to the laboratory results and indicate the vehicle was experiencing minimal movement whilst landed. There is the potential for disturbance of the vehicle while it is landed on the seabed which may influence the taking of measurements. Causes for this include the influence of surface waves and ocean currents as well as drag generated by the attached tether and visual marker buoy.

4.4 Integration of XRF Spectrometer with AUV

An important component of this research is the integration of the XRF system, consisting of an X-ray spectrometer (X-123) and X-ray tube (Mini-X), with the AUV. The off-the-shelf XRF system used for this work is designed for hand-held manual operation in contrast to the requirements of this research that it be operated autonomously in an underwater environment. In order to achieve this, software and hardware components need to be developed. These include drivers to communicate with the devices and an underwater housing. This housing needs to supply power and communications to the XRF system, as well as allowing it to operate in a safe and efficient manner.

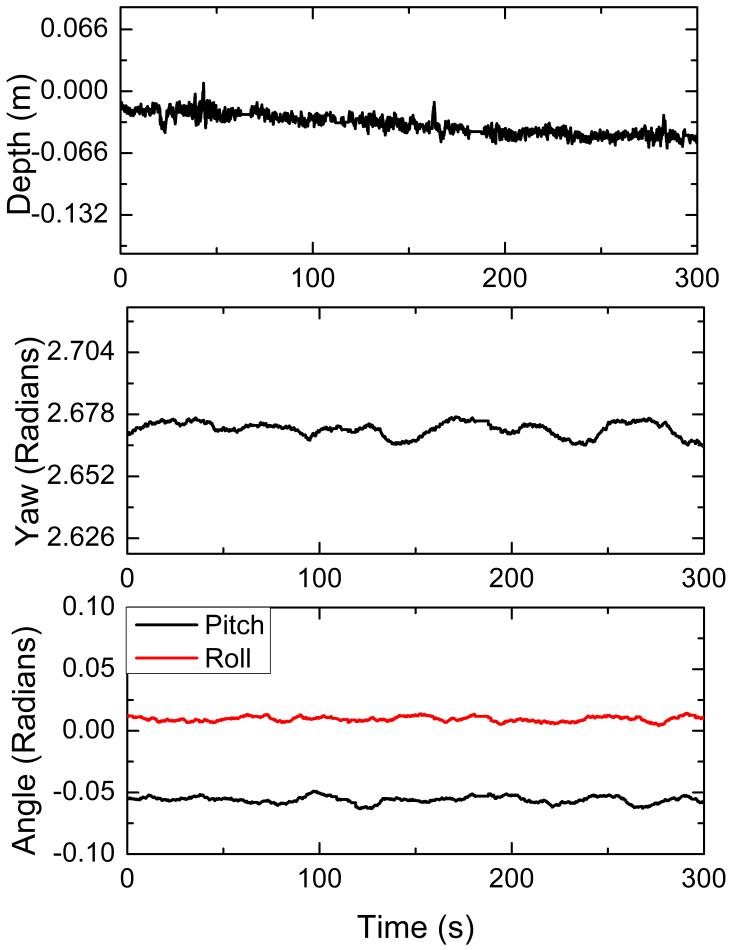

Figure 4.2: Sensor data collected from the vehicle while it was stationary in the laboratory. This provides a comparison for data collected while on the seabed.

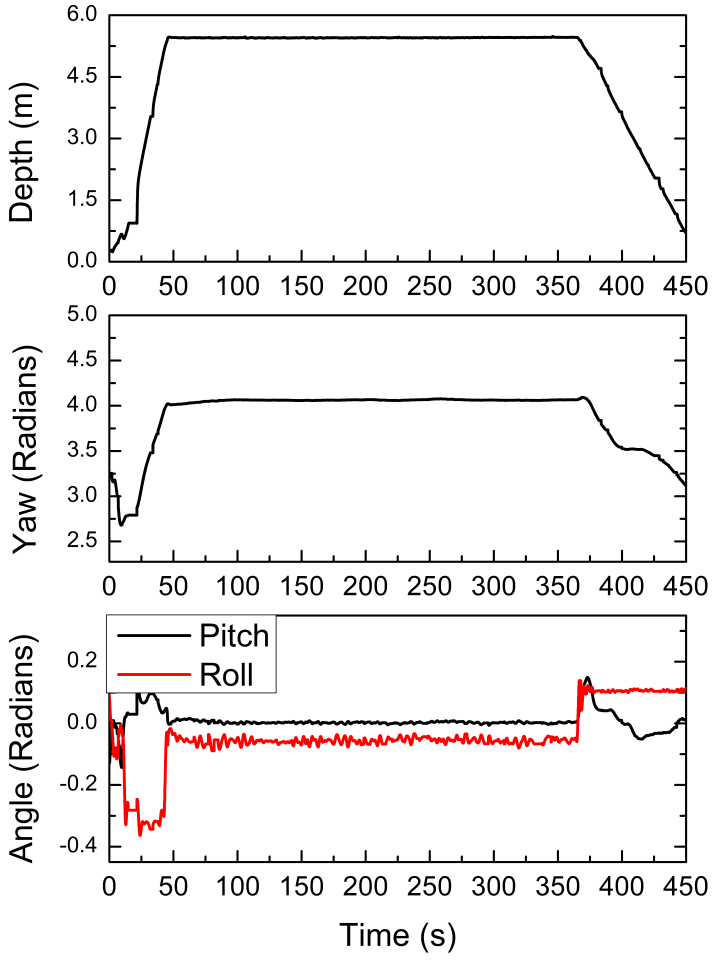

Figure 4.3: Sensor data collected from the vehicle while it was attempting to land on the seabed.

This section discusses the process of integrating the XRF system with the Starbug AUV.

4.4.1 Housing

For the successful operation of the XRF system in the field, a portable housing is required. This needs to be able to be attached to Starbug, be waterproof and large enough to fit the X-ray detector and X-ray tube as well as any additional electronics. The housing consists of an aluminium tube, which has a height of 280 mm and an inside diameter of 110 mm, with a removable cap at each end. The top cap houses the electronics that interface with the detector and X-ray tube which are seated in the bottom end-cap. This bottom end-cap has been discussed in Chapter 3, as it was used for experimental work in the laboratory. This was made out of HDPE due to its strength and low attenuation of X-rays. The housing and mounted spectrometer and X-ray tube are shown in Figure 4.4. Figure 4.5 shows how the detector and emitter are positioned inside the end-cap.

The electronic component of the housing allows the XRF system to be powered and controlled by the AUV.

Incorporated into the end-cap is an electronic circuit that enables the XRF system to be activated in a safe and controlled manner. The electronics for the housing have been designed by John McCulloch of the CSIRO's Intelligent Sensing and Systems Laboratory (ISSL) and were implemented by Trevor Goodwin of the CSIRO Marine and Atmospheric Research (CMAR) division.

The main safety features are two pressure switches which ensure the X-ray tube can only be activated at depth. This prevents accidental activation of the X-ray tube and subsequent exposure to X-rays. These switches have been calibrated to activate at approximately three metres depth. Having two switches introduces redundancy into the system in case of switch failure.

The Mini-X has a hardware interlock that needs to be shorted to allow the production of X-rays. This is normally done using a wire between the two terminals of the interlock. Since the device will be fully contained in the

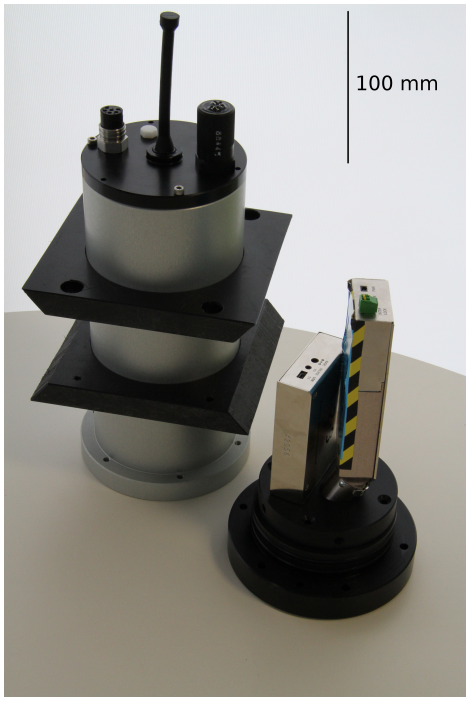

Figure 4.4: The X-ray detector and emitter seated in the end-cap. The X-ray tube is situated in the right side of the end-cap while the detector is in the left side.

housing, the existing interlock system will be inaccessible if urgent deactivation is required. Therefore a method of activating the interlock externally is required. To this end a magnetic reed switch is connected to the interlock terminals attached to the X-ray tube. A magnetic plug can be attached to the top end-cap which activates the reed switch, shorting the interlock, and hence allowing production of X-rays. If the device needs to be quickly deactivated, the plug can be easily removed.

To provide a visual indication of the state of the system a series of LEDs are embedded into the end-cap. The lights indicate whether power is supplied to the system, and also whether the pressure switches are activated. These provide a quick method of determining if the system is safe to approach and give warning that any components of the system may have failed. The electronics visible in the end-cap are shown in Figure 4.6.

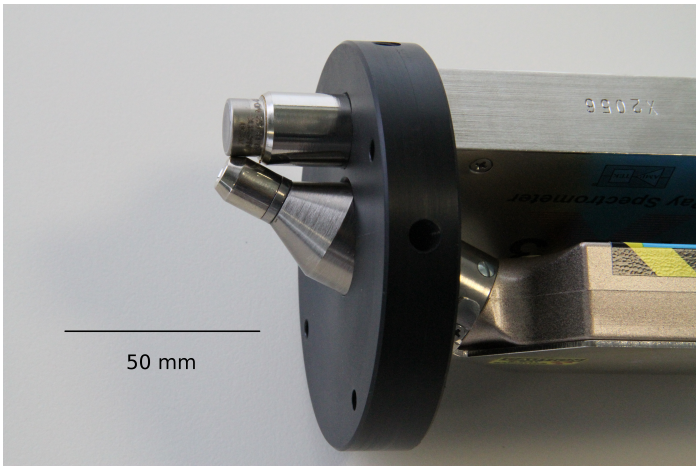

Figure 4.5: The X-ray detector and emitter windows for the two devices, and how they are positioned relative to each other in the end-cap. The X-ray tube is on the bottom.

4.5 Performing an XRF Measurement

Once the vehicle has been identified as landed, the taking of a measurement using the XRF system can commence. This section describes how a measurement is performed from a task level.

At the start of each measurement several parameters relating to the state of the vehicle are recorded. These parameters are the coordinates of the measurement location, depth, and the orientation of the vehicle. This record keeping is an important part of the measurement process.

When the vehicle has been identified as having landed, the X-ray tube is activated by its driver. This driver is called from the task which is responsible for performing the measurement. If an error occurs, and the device is not successfully activated, the task aborts and the vehicle returns to the surface. Potential causes of failure include the vehicle not achieving a sufficient depth to turn the pressure switches on, or the hardware interlock system not being correctly activated. If activation is successful the device will start emitting X-rays at a specified current and voltage. Associated with the XRF data are a number of flags to represent the various stages of the measurement process. One of these flags is updated to reflect the X-ray tube activation. The X-

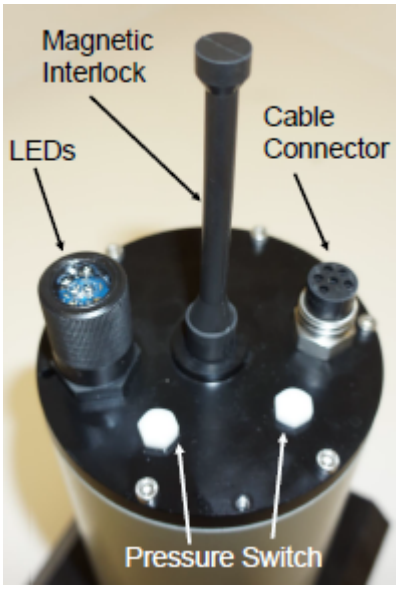

Figure 4.6: The end-cap housing the electronic circuit, with relevant features identified.

ray spectrometer driver, which has been running since the commencement of the mission, detects this flag change and activates the device to begin to detect X-rays and record the spectrum. The measurement is conducted for a predetermined amount of time. After this elapses the X-ray tube is deactivated and another flag is set to communicate to the X-123 driver that the measurement has ceased. The collected spectral data is read from the spectrometer buffer and written to the AUV's data store for automated data analysis. A copy of the spectrum is also written to file for post mission analysis. At this stage the task code instructs the vehicle to ascend to the surface. The measurement is deemed complete from a task point of view when the vehicle reaches the surface and regains a GPS fix. It is then able to proceed to the next sampling site. Subsequent sampling sites can be determined through adaptive sampling described in the next section. The performing of a measurement is outlined in Algorithm 4.2.

Algorithm 4.2 Performing an XRF Measurement

```
Landing procedure has completed.
Activate X-ray tube driver.
if (Device does not activate.) then
  Abort mission
else
  Set flag to indicate commencement of measurement.
end if
while (Perform measurement for predetermined amount of time.) do
  Spectrum is recorded in spectrometer buffer.
end while
Set flag to indicate end of measurement.
Write spectral data to AUV variable store and file.
while (Vehicle does not have GPS fix) do
  Ascend to surface.
end while
```

4.6 Summary

This chapter has discussed the behaviours associated with performing XRF measurements with an AUV. These behaviours are programs which are executed on-board the AUV that use data from engineering sensors, and in the case of adaptive sampling, scientific sensors, to facilitate decision making. These decisions are translated into commands that could be used to control thrusters or activate appropriate sensors. To increase the efficiency of development a simulated environment has been used. This allows behaviours to be tested and debugged in a laboratory environment, reducing the need for potentially time consuming field experiments.

One of the key behaviours is the landing of the AUV on the seabed. To achieve this, the Starbug AUV had to be made negatively buoyant. This removes the reliance on thrusters during the vehicle's descent resulting in lower power consumption and also reducing the disturbance of the sediment layer that is to be analysed. Once a landing is confirmed an XRF measurement can commence by activating the X-ray tube and starting acquisition of spectra with the spectrometer. This chapter has also described the integration of the XRF system with the AUV. This has involved writing drivers to make

the devices compatible with Starbug and its Linux operating system, and the design and implementation of a suitable housing to allow the system to be used underwater. This housing includes several features, such as pressure switches, that allow the device to be activated safely by mitigating the risk of accidental exposure.

Chapter 5

Derwent Estuary Study

5.1 Introduction

This chapter describes the experimental work that has been conducted using the automated XRF measurement and data analysis systems that have been developed throughout this thesis. This involves using an XRF system integrated on-board an AUV to perform automated, in-situ analysis of marine sediments to semi-quantitatively analyse heavy metals. The acquired spectra from the AUV will undergo an automated data analysis process using genetic algorithms which has been described in Chapter 3. The output of this analysis is the intensity (peak area) of the elements present in the observed spectra. These intensities cannot be used to directly compare different spectra obtained from different measurement sites, due to the limitations of performing in-situ measurements using XRF spectroscopy. For results to be directly compared, the geometry of the measurement and sample characteristics needs to be the same and matrix effects need to be taken into account. The observed peaks for each element can be compared to other elements within the same spectrum. This can lead to metrics such as Relative Spectral Area (RSA) or ratios of the RSA to other elements, which can then be used to semi-quantitatively compare different spectra. This can lead to chemical mappings of analysed areas that can identify heavy metal pollution hotspots which can be used to direct further quantitative studies of the area.

Prior to deployment in the field, measurements have been conducted in the laboratory on sediment samples collected from the Derwent which have already undergone quantitative analysis. A comparison of these two datasets has been undertaken which provides an indication of how well the technique correctly identifies those samples with the highest relative heavy metal concentrations. Results from actual in-situ measurements conducted using the Starbug AUV at sites throughout the Derwent are then presented. Analysis and discussion of these will help to evaluate the performance of the technique by demonstrating if it is capable of performing qualitative measurements that are indicative of the heavy metal contamination of a particular site and identifying pollution hotspots present in the surveyed area.

5.2 Previous Studies in the Derwent

There have been numerous studies into heavy metal concentrations in the Derwent (Bloom and Ayling 1977; Butler 2006). These studies analysed heavy metal concentrations in filtered waters, suspended particles, sediments, shellfish and fish. They report the Derwent Estuary is heavily polluted with mercury, cadmium, lead and zinc. An example of a similar survey of heavy metals in an estuarine environment is one in the Gironde Estuary in south-west France (Aurélie Larrose 2010). Like the Derwent, this estuary has high contamination by heavy metals.

In 2009 a report was released by the Derwent Estuary Program (DEP) outlining the state of the Derwent Estuary (Whitehead et al. 2009). This report highlights the severe contamination caused by heavy metals as one of the main environmental concerns facing the Derwent. Results are presented from a sediment mapping survey that was initiated in 2000 by the DEP. This survey involved the analysis of sediment samples taken at 123 sites throughout the Derwent Estuary. These results are compared against existing sediment quality guidelines. These have been published by the Australian and New Zealand Environment and Conservation Council (ANZECC) and are referred to as the National Interim Sediment Quality Guidelines (ISQG) (ANZECC 2000). The concentrations of heavy metals that constitute these

guidelines are shown in Table 5.1.

Metal	**ISQG low**	**ISQG high**
	mg/kg	
Arsenic	20	70
Cadmium	1.5	10
Chromium	80	370
Copper	65	270
Lead	50	220
Mercury	0.15	1
Nickel	21	52
Silver	1	3.7
Zinc	200	410

Table 5.1: National sediment quality guidelines for heavy metals (ANZECC 2000).

If the ISQG low values are exceeded then there is a 10% probability of that particular heavy metal causing adverse biological effects. In the event that the high values are exceeded this probability rises to 50%.

The results of the DEP's study are shown in Table 5.2.

Metal	**< ISQG low**	**> ISQG low but < ISQG high**	**> ISQG high**
		%	
Arsenic	79	14	7
Cadmium	36	52	12
Copper	74	23	4
Lead	23	38	39
Mercury	1	34	65
Zinc	32	20	48

Table 5.2: Proportion of Derwent Estuary sediments that meet or exceed sediment quality guidelines (Whitehead et al. 2009).

These results show that the majority of sediments sampled do not meet the ISQG. Of particular concern is the concentration of mercury, lead, zinc and cadmium. The study identified the middle region of the estuary as being particularly contaminated. This highlights the extent of heavy metal pollution in the sediments found in the Derwent Estuary.

5.3 Initial Laboratory Results

Before results were collected in the field, a number of experiments were conducted in the laboratory. These served to provide familiarity with the spectral acquisition and analysis procedures. The analysis has been done on a set of 15 samples, provided by the University of Tasmania's Centre for Ore Excellence, which have been collected from a core taken from the Derwent river. Each sample is representative of a five centimetre section of the core, from 0 cm to 75 cm. A section of each sample has been prepared and then undergone a quantitative analysis. This analysis has been undertaken by the Centre for Ore Excellence. The resulting data is the concentrations of detected elements in parts-per-million.

These samples have also undergone analysis using the technique developed in this thesis. The resulting dataset from this analysis is the RSA for each element present.

This provides an interesting opportunity to compare quantitative data with the semi quantitative RSA results obtained using the technique developed in this thesis. This is an important step in testing the hypothesis that the proposed technique of performing XRF analysis can distinguish between samples based on their heavy metal concentration.

Each spectrum was acquired in the laboratory over a period of five minutes and analysed using the developed genetic algorithm. The RSA of the heavy metals present in the spectra has been used as the metric of interest for the obtained results. The comparison of the two datasets is shown in Figure 5.1. The quantitative results show the concentration of the heavy metals tends to increase with core depth, with a peak at the sample representing 55 - 60 cm, until depths 65 - 75 cm where the lowest concentrations are recorded.

The semi-quantitative analysis performed in the laboratory show the same general trend as the quantitative data set, with the relative percentage of heavy metals increasing with core depth with a sudden decrease in the heavy metal concentrations for the last two samples. The samples with the highest detected heavy metals are at core depths 55-65 cm. This compares favourably to the region of the core that the quantitative results identify as containing

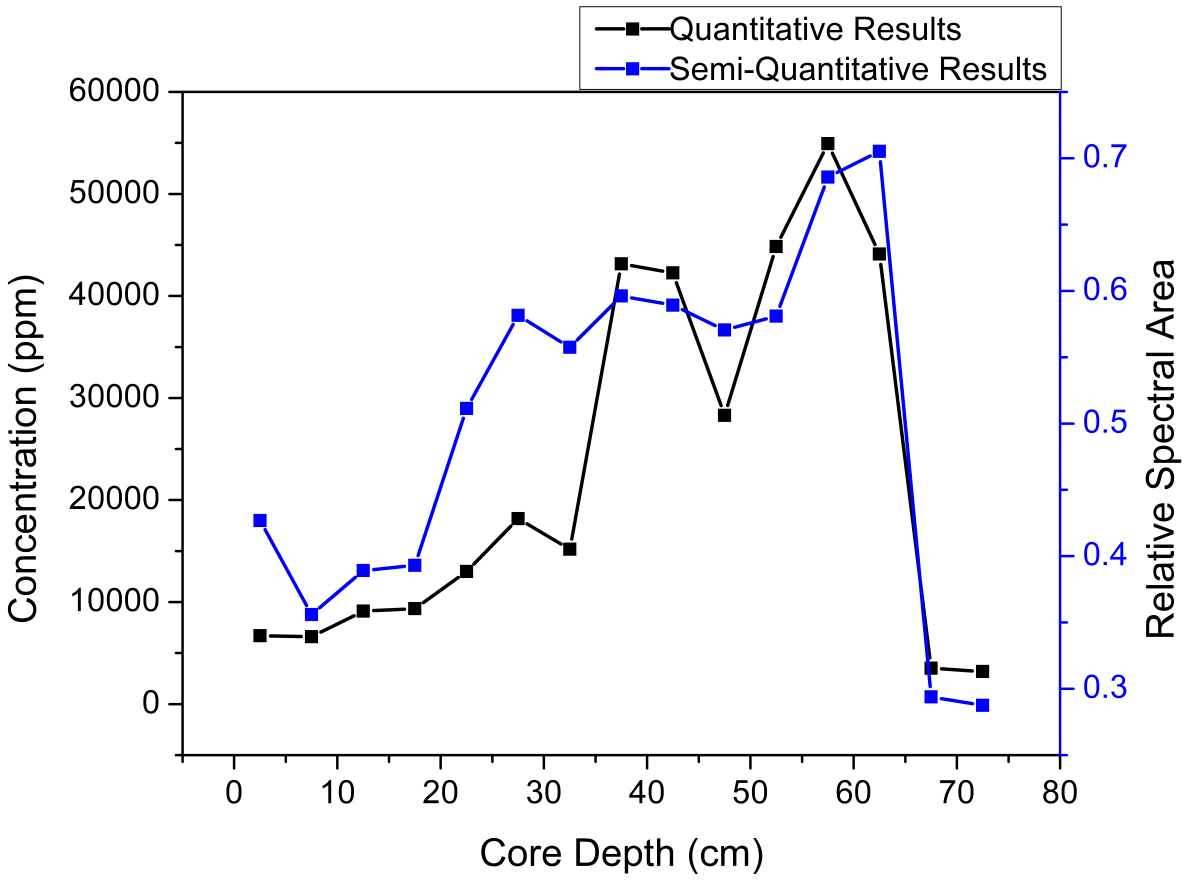

Figure 5.1: Comparison of the results from the quantitative and semi-quantitative analysis of sediment samples. This shows the combined relative spectral area of the heavy metals, lead and zinc.

the highest concentrations of zinc and lead at depths 50-65 cm indicating some correlation between the two data sets. There are some discrepancies present between the two datasets. There are several possible explanations for this. There may be variations in elemental concentrations throughout each sample which could be detected by analysing different sections in the two analyses. The quantitative results have had the matrix effects corrected for through calibration processes. The results obtained for this thesis have not been corrected for these effects, resulting in peak intensities that may be affected by other elements present. This causes the area under the peaks in the obtained spectra to be over or underestimated. The RSA metric is also not a direct measure of the concentration of each element. It is calculated by looking at the percentage contribution of each element to the overall spectral area. Large RSA values do not necessarily translate to large concentrations. It is possible for a given element to have a large proportion of the measured area of all detected elements, but still have a low physical concentration. This can be due to the presence of other elements in the sample that are not detected in the analysis. The RSA is used as a metric to identify those measurements which may be of interest and contain high levels of heavy metals. The results presented in this section show this hypothesis is a sound one by demonstrating the ability of the technique to produce semi-quantitative results that are indicative of the measured amounts of heavy metals present allowing the detection of hotspots from a set of analysed samples such as those performed in a laboratory or in-situ measurements performed in the field.

5.4 Sampling in the Field

This section presents results from measurements taken using an XRF system attached to an AUV at sites throughout the Derwent Estuary. These measurements were performed and the collected spectra analysed according to the methods that have been discussed throughout this thesis. Analysis of these results will help to evaluate the performance of the technique and whether they are indicative of the sediment found at each site.

5.4.1 Site Selection

Measurements were conducted in three distinct regions in the Derwent Estuary which are shown in Figure 5.2.

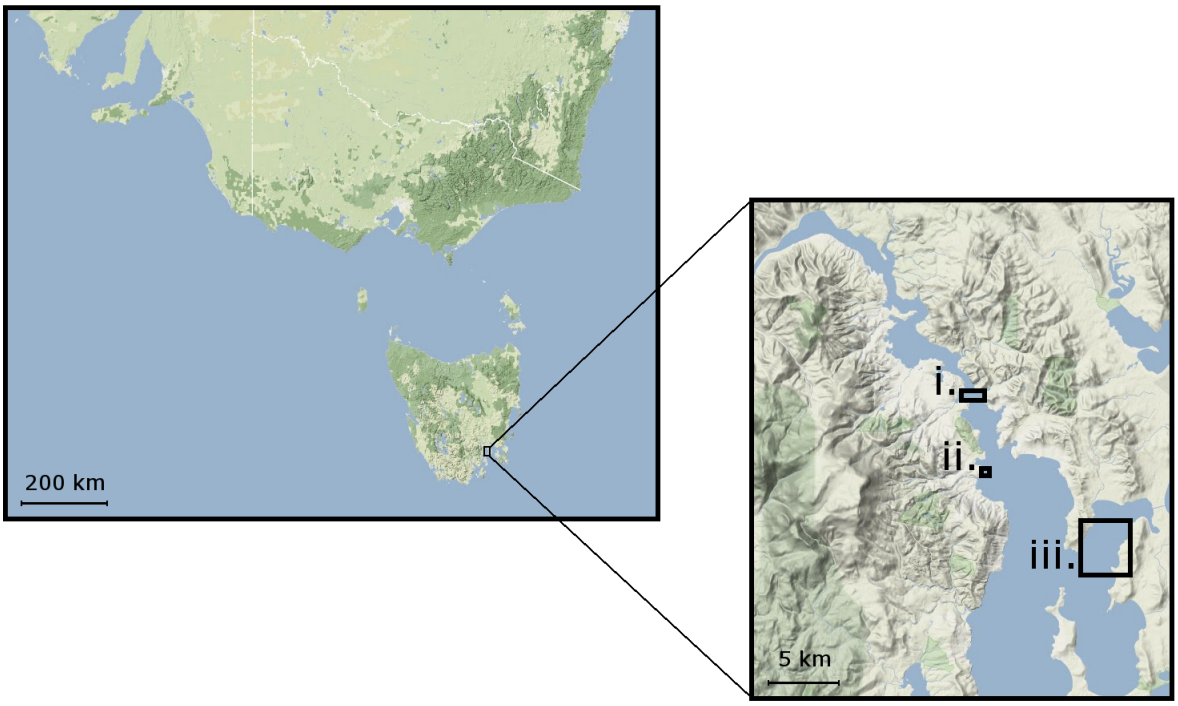

Figure 5.2: Map of the Derwent Estuary in southern Tasmania showing the locations of the three regions where in situ measurements will be performed.

The regions have been selected according to several factors; results from previously conducted studies, safety and access issues. Region **i** is located to the north of the estuary in the vicinity of industrial sites. Previous studies into heavy metal contamination in this area report the highest readings obtained are from this region. Located south is region **ii** which is an area that is frequently used for Starbug testing purposes with deployment possible from the shore. Region **iii** is in the south east of the Derwent estuary in an area known as Ralph's Bay. This area was chosen due to the fact it does not experience heavy shipping traffic, allowing for safer deployment of the AUV,

and also because previous studies suggest variability in the concentrations of heavy metals may be observed. The measurement sites used are listed in Table 5.3.

Site ID	Location Lat, Long
Region i	
A	-42.841915 147.336845
B	-42.842789 147.336752
C	-42.843381, 147.325019
D	-42.84238, 147.32233
Region ii	
E	-42.889044, 147.33862
F	-42.888990, 147.33871
Region iii	
G	-42.953516, 147.428676
H	-42.945979, 147.433367
I	-42.94311, 147.441817
J	-42.93736, 147.449902
K	-42.943661, 147.419892
L	-42.939847, 147.426044
M	-42.938917, 147.429065
N	-42.935343, 147.435964
O	-42.935663, 147.441886
P	-42.930358, 147.446664
Q	-42.927088, 147.451641
R	-42.942883, 147.420794
S	-42.948928, 147.417599
T	-42.932163, 147.43642
U	-42.931466, 147.437199

Table 5.3: A list of the sites where measurements have been performed.

5.4.2 Performing Field Measurements with AUV

The measurements conducted in regions **i** and **iii** were performed from a support vessel. The boat navigates to the measurement area and the AUV is deployed. Sites in region **ii** were conducted from shore. Figure 5.3 shows the AUV with XRF system attached prior to deployment.

A mission file specifies the locations where measurements are to be performed.

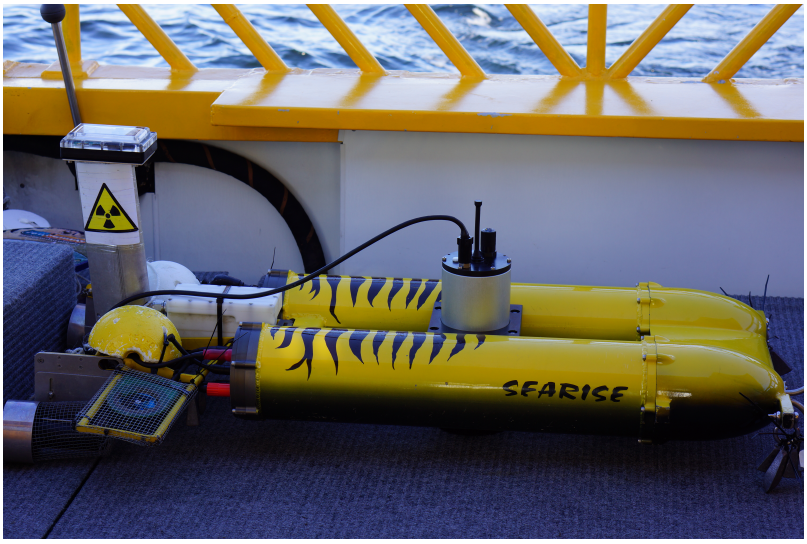

Figure 5.3: The housing attached to the AUV prior to deployment.

Each measurement was conducted for five minutes to achieve a sufficient signal-to-noise ratio. Prior to analysing the measured spectral data it is important to ensure the measurement was conducted in conditions conducive to good quality results. An ideal measurement scenario has the vehicle stationary for the duration of the measurement. Inadequate contact with the seafloor, which could be caused by the vehicle moving once landed, could degrade the quality of the acquired spectrum. Through analysis of collected engineering data it is possible to identify those measurement attempts that potentially yield inferior results. Relevant data are the standard deviation for the roll, pitch, yaw and depth for the duration of the measurement. High values may indicate the vehicle was not stationary during spectrum acquisition and therefore data may not be of sufficient quality. Table 5.4 shows the relevant engineering data for each measurement location.

This table shows low standard deviations for depth, roll, pitch and yaw for the majority of the measurements performed that are similar to those obtained from the stationary vehicle in the laboratory. This indicates that the vehicle remained stationary during spectra acquisition. The measurement corresponding to site C has a large standard deviation value for the yaw of

Site ID	Depth Std. Dev. m	Pitch Std. Dev.	Roll Std. Dev. Degrees	Yaw Std. Dev.
Region i				
A	0.010	0.110	0.237	0.342
B	0.011	0.181	0.164	1.100
C	0.006	0.154	0.232	7.022
D	0.006	0.163	0.005	0.333
Region ii				
E	0.011	0.121	0.243	0.545
F	0.023	0.133	0.185	0.583
Region iii				
G	0.011	0.152	0.278	0.195
H	0.015	0.128	0.126	0.190
I	0.015	0.167	0.303	0.382
J	0.014	0.149	0.166	0.298
K	0.014	0.148	0.183	0.812
L	0.006	0.138	0.111	0.624
M	0.010	0.197	0.160	1.038
N	0.011	0.108	0.119	0.185
O	0.009	0.102	0.196	0.686
P	0.006	0.143	0.106	0.398
Q	0.006	0.150	0.225	0.515
R	0.007	0.137	0.172	0.255
S	0.022	0.246	0.827	0.648
T	0.014	0.131	0.126	0.204
U	0.015	0.295	0.145	0.295

Table 5.4: The engineering data collected during the taking of XRF measurements.

the vehicle which may indicate excessive movement while landed, and flags the measurement as of potentially bad quality. Analysis of the recorded yaw data (shown in Figure 5.4) shows that the vehicle rotated approximately 0.40 radians (23 degrees) over the duration of the measurement. This plot shows time as "Epoch". This is a measurement of time that is common in computer science. It refers to the amount of seconds that have elapsed since midnight (Coordinated Universal Time) January 1 1970. This is used as a time stamp for all sensor data from the robotic platform Starbug.

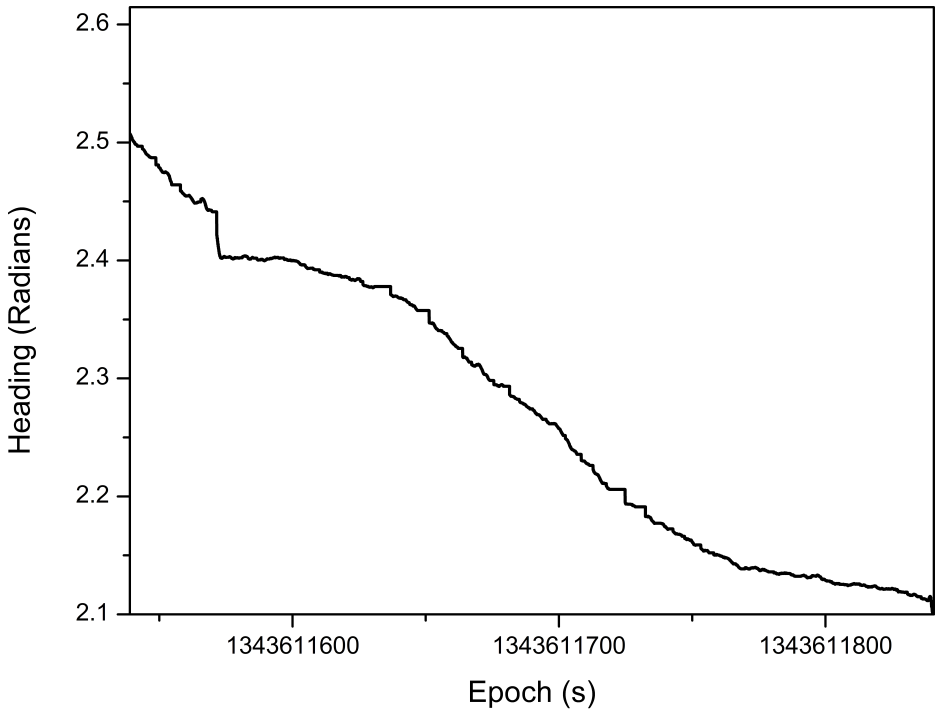

Figure 5.4: Yaw data during the taking of an XRF measurement at site C.

To determine if the spectrum associated with this measurement is of sufficient quality to use in the analysis it is compared against one collected with satisfactory engineering data (site D). There are approximately 240 m between the two sites. This is shown in Figure 5.5.

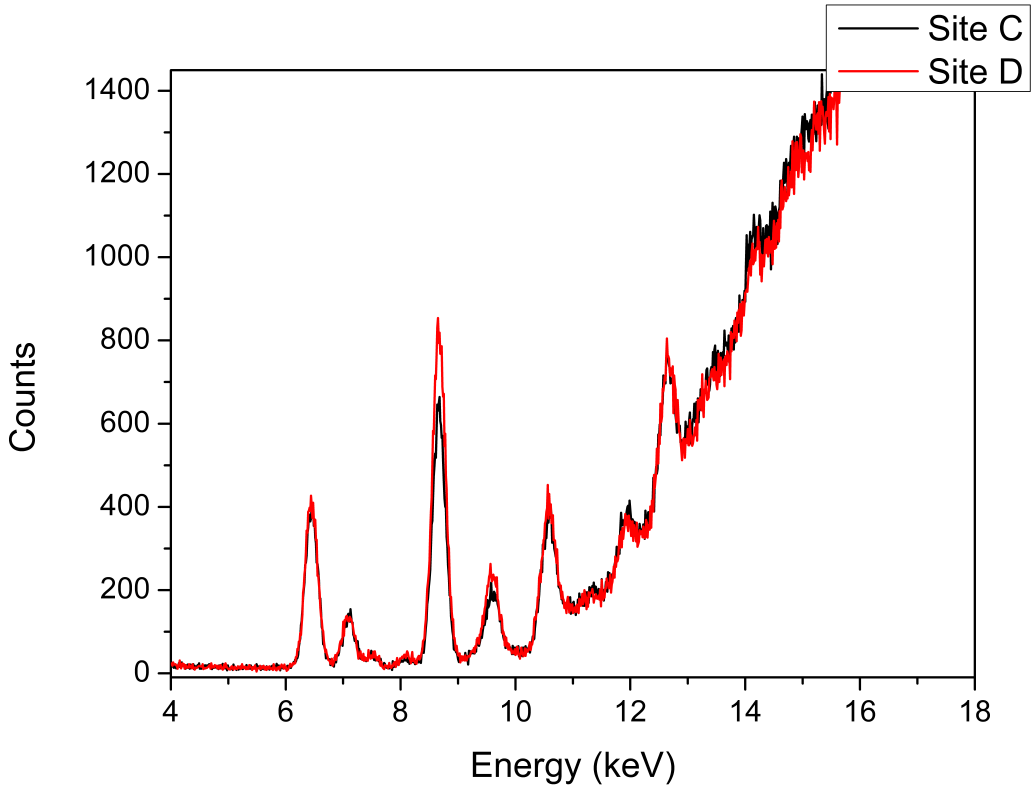

Figure 5.5: Comparison of spectrum acquired from site C and site D.

Peaks from elements present in marine sediment are evident in both spectra and the levels of counts acquired are similar. This suggests contact with the seafloor was maintained throughout the measurement despite the vehicle rotation indicated by the engineering data.

5.4.3 Results of Field Measurements

Figures 5.6 and 5.7 show two examples of spectra that have been obtained from analysis performed underwater. They are site D from region **i** and site U from region **ii** respectively. These show the variability that has been detected in the study. They have undergone automated data analysis, and the fitted peaks are shown.

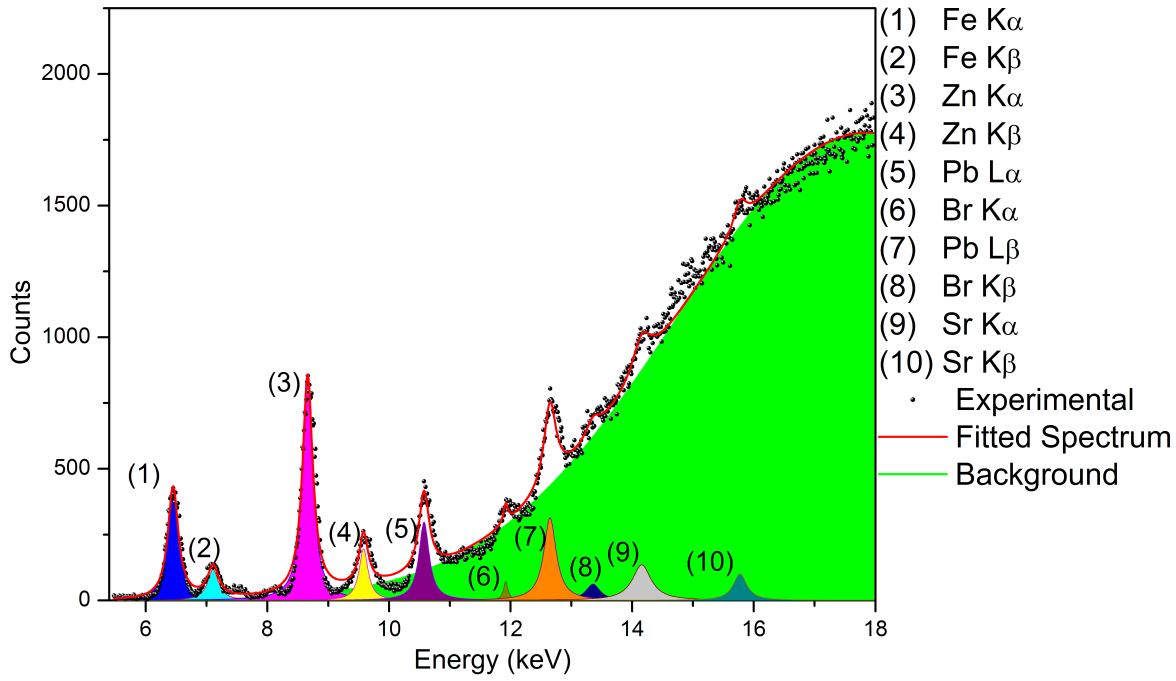

Figure 5.6: Example of a fitted spectrum obtained by analysing sediment at measurement site D.

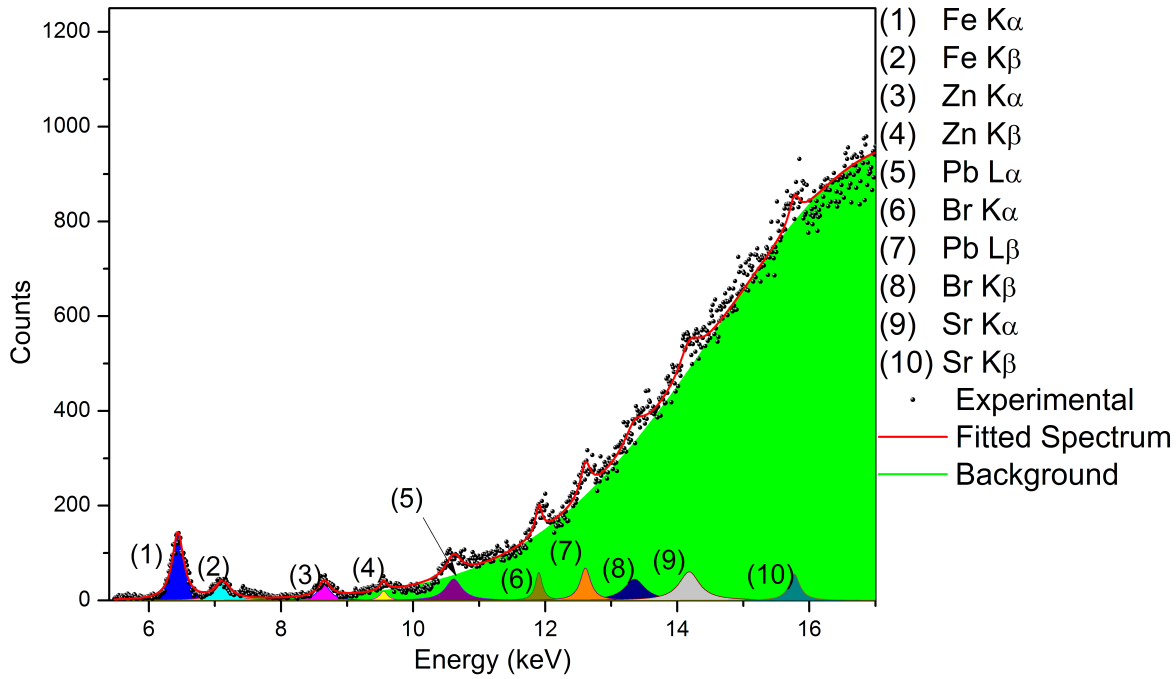

Figure 5.7: Example of a fitted spectrum obtained by analysing sediment at measurement site U.

The results from the measurements performed are summarised in Table 5.5. This table shows the RSA for each element present as well as the ratio of the heavy metal elements (zinc and lead) to another main constituent of the sampled marine sediments, iron. The ratio metric is useful as it removes the influence of other elements that may be constituents of the seawater and not the sediment.

Site ID	**Depth m**	**Zn**	**Pb**	**Fe**	**Other**	**(Zn+Pb)/Fe**
			%			
Region i						
A	7.46	17.71	31.22	20.89	30.18	2.34
B	7.01	12.67	21.94	16.17	49.21	2.14
C	4.79	30.68	26.67	21.25	21.39	2.70
D	7.08	33.9	27.03	18.05	21.03	3.38
Region ii						
E	4.56	7.25	22.51	21.26	49.31	0.71
F	7.59	7.89	27.47	21.15	45.70	0.71
Region iii						
G	13.57	7.565	6.849	21.8	63.79	0.66
H	11.95	8.742	7.097	29.78	54.38	0.53
I	9.91	5.987	6.835	24.68	62.5	0.52
J	8.41	0.819	0.583	6.06	92.54	0.23
K	21.42	7.258	12.82	25.29	54.63	0.79
L	21.01	5.936	13.56	23.4	57.1	0.83
M	13.68	8.441	16.59	27.78	47.19	0.90
N	11.28	5.435	15.52	18.11	60.93	1.16
O	10.34	4.188	16.49	17.76	61.56	1.16
P	10.43	6.466	18.07	21.35	54.11	1.15
Q	7.44	1.716	9.453	12.33	76.5	0.91
R	23.58	6.68	15.08	24.44	53.8	0.89
S	16.16	5.387	3.032	18.06	73.52	0.47
T	9.41	4.727	13.15	23.92	58.2	0.75
U	8.95	5.586	17.84	23.45	53.13	1.00

Table 5.5: The results obtained from performing in situ XRF measurements in the Derwent Estuary.

This table shows the associated location and depth data for each measure-

ment site. The location for each site is measured by the AUV's GPS units while on the surface, prior to commencing descent to the seabed. Because there is no horizontal thrust applied during the descent phase, the vehicle's location is not altered by dead reckoning while it is submerged performing the measurement. However the vehicle is likely to move away from this location during its descent due to a variety of issues, including the influence of current and wave action. Therefore the location information for each measurement site should be treated as an approximation. The depth data has not been corrected for the tide and represents the actual depth recorded at the time of measurement. The depth sensor readings have been averaged for the duration of the measurement to account for wave action.

The data shown in Table 5.5 can be visually shown in a ternary plot (Figure 5.8). Ternary plots are used to show the composition of a system comprising of three variables. The proportions of the variables must sum to a constant, in this case 1.0. The position of each data point represents a value on each of the three axes. The values can be read to determine the individual proportions of each variable for that data point. This shows the proportions of heavy metals, iron and other elements for each measurement and can be used to identify distinct groups within a dataset that share similar elemental compositions.

The acquired data shows that the measurements associated with region **i** have the highest RSA of heavy metal. Region **i** was located in close proximity to industrial sites and the highest readings from previous studies have been located in this area. Site D recorded the highest spectral area attributable to heavy metal elements. The calculated spectral area of heavy metals is over 3 times that of iron. This indicates the presence of anthropogenic sources of heavy metal contaminants. It also suggests that heavy metal discharge from industrial sites impacts significantly on the sediments in the immediate area as opposed to being transported by hydrological processes to other regions before settling out. Two measurements have been performed at region **ii** and are shown to be of similar relative compositions. A total of 15 measurements were conducted within region **iii** in Ralph's Bay. The results do not have significant variability and there are no major heavy metal hotspots within

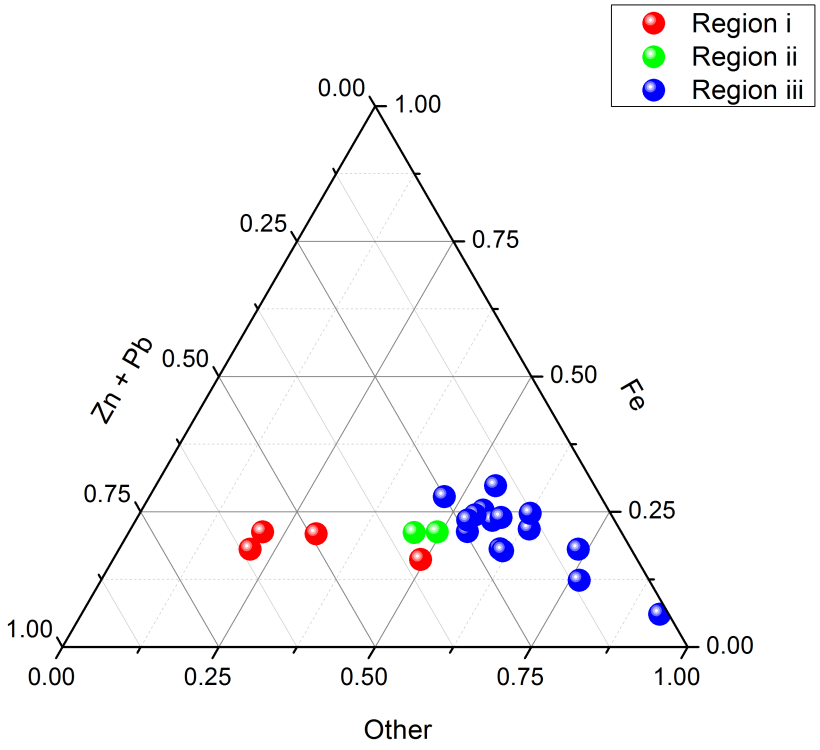

Figure 5.8: Ternary representation of the obtained data. This shows the RSA for the heavy metals, zinc and lead, iron as well as the other elements present, bromine and strontium.

the region. The measurement with site identification **I** has shown little RSA of heavy metals and Fe, with 92.5% of the observed spectral area attributed to the elements designated other, Br and Sr. This unique result may be a genuine representation of the site or may indicate an erroneous measurement. The engineering data associated with this measurement indicates that the vehicle was stationary for the duration of the measurement. However the seabed in this location may not uniformly flat, and the XRF sensor not placed in contact with the sediment. This would result in a spectrum of the surrounding seawater being collected explaining the low reading from the analysis. Further investigation of this area may be required with additional measurements.

One potential method of interpreting these results could be to generate an interpolated map showing the distribution of heavy metals that have been detected. It is worthwhile to reaffirm the reason why this interpretation does not make sense for these results. The metric being used to identify regions of interest is the RSA of heavy metals present in each measurement. This is calculated by comparing the intensity of the peaks associated with one element with the total intensity of the entire spectrum. This calculation is dependent on each specific measurement. It is not possible to directly compare measurements due to the different conditions, such as other elements present in the sediment, measurement geometry, particle size and moisture content, at each site affecting the detected intensities of the elemental peaks. The RSA metric has been used as an attempt to identify those sites that potentially contain high heavy metal levels and warrant further investigation using quantitative methods.

5.5 Summary

This chapter has presented results obtained using the XRF measurement and data analysis techniques that have been developed throughout this thesis. Analysis of these results is an important step towards evaluation of the system. Prepared sediment samples have been analysed in the laboratory, and compare favourably to results obtained through full quantitative analy-

sis. This indicates that the measurement and analysis technique can provide an adequate method of semi-quantitative sediment analysis.

The culmination of the research presented in this thesis was the performing of in situ measurements underwater using the XRF system with an AUV. A total of twenty measurements were conducted in three regions throughout the Derwent Estuary. The RSA of heavy metals, zinc and lead, as well as iron, bromine and strontium concentrations of these measurements have been calculated from obtained spectra using the developed automated data analysis algorithm to provide immediate feedback of measurements. Results have shown that the highest levels of heavy metals encountered were in close proximity to industrial sites. This result is supported by previous studies presented in literature. Good spatial correlation has been observed from results within the distinct regions. This demonstrates the ability of the technique to detect spatial variability in relative heavy metal RSA that is indicative of the actual elemental composition of the sediment layer.

Chapter 6

Conclusion

The goal of this thesis was to develop a novel technique capable of performing automated in situ X-Ray Fluorescence (XRF) spectroscopy of marine sediments for the analysis of heavy metal pollution. This is a particularly topical area for the Derwent Estuary in south-east Tasmania as it has some of the highest levels of contamination by heavy metals in the world. Currently marine sediments are sampled using manual techniques which are expensive, time consuming and may potentially disturb the surface sediment layer which is the most bio-available. This chapter will provide a summary of the work carried out to undertake this research, which resulted in the development of the new technique, and results obtained in the field. Some limitations will be discussed and potential future research that could originate from the work presented here will also be explored.

6.1 Research Contribution

The main contribution of this work is the development and implementation of an alternative technique for the analysis of marine sediment chemistry. This technique provides the capability to perform a semi-quantitative in situ assessment of heavy metal contamination in an autonomous manner. This has been achieved through the following key research components:

1. This research uses a commercially available portable XRF system com-

prising of an X-ray spectrometer and X-ray tube and an AUV platform developed by the CSIRO called Starbug. There has been a significant amount of work in integrating the XRF system with the AUV to allow measurements to be performed underwater. Software has been developed which allows the AUV computer to autonomously control the devices and store spectral data in accordance with Starbug's data structure for sensor variables. A custom housing has been designed that allows the XRF system to be attached to the vehicle. This consists of a waterproof aluminium cylinder with a removable cap at either end. The spectrometer and X-ray tube are seated in the downwards-facing end-cap. The material of this end-cap presented an important design choice that influenced the success of the approach. It needed to be strong enough to withstand contact with a potentially abrasive seabed and also features a thin window through which X-rays could pass with minimal attenuation. HDPE was decided upon as it provided the strength required and allowed X-rays to pass through with acceptable levels of attenuation. The top end-cap houses electronics that are used to interface the XRF devices with Starbug. Communications and power to the housing are provided via a port on Starbug's hull that is configured for USB devices. Because of the X-ray tube producing potentially harmful X-rays the electronics incorporate safety features that minimise the risk of accidental exposure. Pressure switches restrict activation of the X-ray tube until it is at a safe depth and it has a magnetic interlock which can allow immediate deactivation of X-ray production. A series of LEDs indicate the current state of the system and can alert the operator to a potential malfunction.

2. To allow the AUV to make sense of the spectral data it acquires, an automated method of performing data analysis has been implemented. This uses genetic algorithms to curve-fit the data. Each elemental peak present in the spectrum can be approximated with a Lorentzian function. The curve parameters for all expected elements are fitted through an iterative process. Bounds for these parameters are based on the

known theoretical energy of each element and through an initial analysis of the acquired data, increasing the accuracy of the fitting. Aside from the elemental peaks, the peak associated with bremsstrahlung radiation needs to be fitted to account for its influence on observed peak intensities. The genetic algorithm stops when the peak parameters of subsequent generations have negligible variance. The parameters from the optimal solution are used to calculate the area beneath each peak and therefore the relative spectral area of each element which can be used as a semi-quantitative measure of their concentration. This has provided a quick and accurate method of performing data analysis in real time on-board an AUV to facilitate an adaptive sampling approach.

3. The AUV demonstrates behaviours through following programmed tasks. These use data acquired by the vehicle's sensors to perform actions using the thrusters or other devices. A key behaviour required for this work was the landing of the AUV on the seabed. This was achieved through weighting the vehicle so it was negatively buoyant reducing the reliance on the thrusters. Using the thrusters to land a positively buoyant vehicle and keep it in place on the seabed can disturb the sediment layer as well as consume the limited power supply. When the vehicle has sensed it has finished descending, XRF measurement can commence. While the AUV is seated on the seafloor it can be susceptible to external forces causing it to move. Movement during a measurement can impact on the quality of the sensed data. Therefore it is important to record variables relating to the vehicle's state. These can be used to determine whether there was significant movement during the measurement and flag data as being of potentially poor quality.

This thesis has successfully demonstrated XRF spectroscopy of sediment chemistry underwater. This has been done autonomously, removing the need for direct human involvement with performing the measurements. This represents an evolution of previous work involving in situ measurements performed manually (Wogman et al. 1975; Wogman and Nielson 1980). An automated data analysis technique is used immediately on-board the AUV to allow a

semi-quantitative assessment of each measurement site to be performed. This work can be seen as the precursor to performing adaptive sampling.

6.2 Summary of Results

Prior to deployment in the field, this technique was applied on 15 sediment samples in the laboratory. These were taken from a core sample from the Derwent Estuary and had already undergone a quantitative analysis, enabling a comparison with the results obtained using the developed data analysis method. The technique correctly identifies the samples that have the highest concentrations of heavy metals, zinc and lead, according to the quantitative dataset, as well as the lowest. This indicates that the relative concentrations for the heavy metals detected compare favourably to results from a more quantitative measurement process.

The culmination of the development of the sampling technique has been its deployment in the field. A total of 21 measurements were conducted at three distinct regions throughout the Derwent Estuary. The elements identified are zinc and lead, which are the heavy metals the study is focusing on, iron, strontium and bromine which is likely from the surrounding seawater. The highest detected levels of heavy metals were located at measurement sites adjacent to industrial sites. This suggests that these sites act as an anthropogenic source of heavy metals, and the contaminants effect nearby sediment rather than being transported further afield.

These results have shown the technique that has been developed throughout this thesis is capable of detecting semi-quantitative spatial variation in heavy metal levels.

6.3 Limitations

One of the main limitations of this technique is the inability to perform a full quantitative analysis. The main reason for this is the matrix effects described in Chapter 3. This is where other elements in a sample influence the

observed intensity of characteristic X-rays produced by a particular element. Correction of these effects requires extensive calibration and experimental work that is beyond the scope of this thesis. Other factors include the particle size of the sample and geometry of the measurement, which are difficult to address in performing in situ measurements.

Another limitation concerns not being able to know when the XRF sensor has been in contact with the seabed. Currently engineering data is used to evaluate whether the vehicle was stationary for the duration of a measurement. If the collected sensor data indicates the vehicle was moving during the measurement it could indicate that the sensor was not in contact with the sediment and instead analysing the surrounding seawater. However it is possible for the vehicle to be stationary yet still have insufficient contact. This could be because of irregularities in the surface of the seabed. Being able to know whether contact had been made would be useful for deciding if spectra that have minimal peaks associated with sediment are valid. One potential method of mitigating this is to install a contact sensor on the base of the housing that could indicate when it is positioned correctly on the seabed.

6.4 Further Work

This research has laid the foundation for further work in increasing the intelligence of performing autonomous measurements. Of particular interest is the inclusion of scientific sensor data in the decision making process of robotic platforms. The implementation of adaptive sampling to supplement an XRF measurement mission could increase its scientific return. This will allow subsequent measurement sites to be chosen depending on previous results. Sites that have yielded high relative concentrations of heavy metals can be identified on-board the robot using the automated data analysis technique that has been described. This could result in additional measurement sites being created in the vicinity of regions of interest.

One potential use for this novel technique is to guide a full quantitative survey to those locations that may yield high levels of heavy metals. This could be achieved through complementing the current method of obtaining

samples for laboratory analysis with measurements performed by the XRF system on-board the AUV. Instead of relying on predetermined measurement sites, the AUV could quickly perform semi-quantitative analysis within regions and use the results to suggest potential locations to obtain samples from.

The successful implementation of XRF spectroscopy underwater has proven the feasibility of performing in situ analysis of sediment chemistry underwater with an AUV. Further scientific opportunities may be found in exploring alternative techniques. Potential techniques include Mössbauer spectroscopy and Laser Induced Breakdown Spectroscopy (LIBS). Mössbauer spectroscopy can be used to perform an automated in-depth analysis of the iron that has been detected in the estuary. This can be used to identify the type of iron bearing mineral present and may indicate its source, either industrial or natural. LIBS uses a laser to ablate a sample and perform elemental analysis through observing the optical emission of the resulting plasma. Previous research into performing LIBS underwater has highlighted some unique research challenges (Pichahchy et al. 1997; Michel et al. 2006; Lazic et al. 2007). These are mainly related to issues with using a laser underwater to ablate the sample. Some of the research that has been undertaken in this thesis could be reapplied to these techniques. The automated data analysis that has been developed using genetic algorithms can be used on the data collected using these alternative techniques. This can be done through the redefinition of the peak parameters and fitness function.

References

Ahonen, H., de Souza, P. A. and Garg, V. K. (1997), 'A genetic algorithm for fitting lorentzian line shapes in mössbauer spectra', *Nuclear Instruments and Methods in Physics Research Section B: Beam Interactions with Materials and Atoms* 124(4), 633 – 638.

Amptek (2012), 'Amptek company website'. `http://www.amptek.com`.

An, E. (2003), A comparison of auv navigation performance: a system approach, *in* 'Proceedings - Oceans, 2003, San Diego, USA', Vol. 2, pp. 654 –662 Vol.2.

Ansari, T., Marr, I. and Tariq, N. (2004), 'Heavy metals in marine pollution perspective-a mini review', *Journal of Applied Sciences* 4, 1–20.

ANZECC (2000), *Australian and New Zealand Guidelines for Fresh and Marine Water Quality*, Australian and New Zealand Environment and Conservation Council.

Aurélie Larrose, Alexandra Coynel, J. S. G. B. L. M. E. M. (2010), 'Assessing the current state of the gironde estuary by mapping priority contaminant distribution and risk potential in surface sediment', *Applied Geochemistry* 25(12), 1912 – 1923.

Beckhoff, B., Kanngieber, B., Langhoff, N., Wedell, R. and Wolff, H. (2006), *Handbook of Practical X-Ray Fluorescence Analysis*, Springer Berlin Heidelberg New York.

Bellingham, J. G. and Rajan, K. (2007), 'Robotics in remote and hostile environments', *Science* 318(5853), 1098–1102.

Bloom, H. and Ayling, G. (1977), 'Heavy metals in the derwent estuary', *Environmental Geology* 2(1), 3–22.

Bowen, A., Yoerger, D., Taylor, C., McCabe, R., Howland, J., Gomez-Ibanez, D., Kinsey, J., Heintz, M., McDonald, G., Peters, D., Fletcher, B., Young, C., Buescher, J., Whitcomb, L., Martin, S., Webster, S. and Jakuba, M. (2008), The nereus hybrid underwater robotic vehicle for global ocean science operations to 11,000m depth, *in* 'Proceedings - Oceans 2008, Quebec City, Canada', pp. 1 –10.

Breen, J., de Souza, P., Timms, G. and Ollington, R. (2011), 'Onboard assessment of xrf spectra using genetic algorithms for decision making on an autonomous underwater vehicle', *Nuclear Instruments and Methods in Physics Research Section B: Beam Interactions with Materials and Atoms* 269(12), 1341 – 1345.

Breen, J. and McCulloch, J. (2012), Real time visualisation of sensor data for an autonomous underwater vehicle via a wi-fi buoy, *in* 'Proceedings - Oceans, 2012, Yeosu, South Korea', pp. 1 –3.

Brunetti, A. (2013), 'A fast fine-grained genetic algorithm for spectrum fitting: An application to x-ray spectra', *Computer Physics Communications* 184(3), 573 – 578.

Brunetti, A. and Golosio, B. (2001), 'Fit of edxrf spectra with a genetic algorithm', *X-Ray Spectrometry* 30(1), 32–36.

Butler, E. (2006), The tail of two rivers in tasmania: The derwent and huon estuaries, *in* P. Wangersky, ed., 'Estuaries', Vol. 5H of *The Handbook of Environmental Chemistry*, Springer Berlin / Heidelberg, pp. 1–49. 10.1007/6985022.

Camilli, R., Bingham, B., Jakuba, M., Singh, H. and Whelan, J. (2004), Integrating in-situ chemical sampling with auv control systems, *in* 'Proceedings - Oceans, 2004, Kobe, Japan', Vol. 1, pp. 101 – 109 Vol.1.

Castellano, A., Buccolieri, G., Quarta, S. and Donativi, M. (2006), 'Portable EDXRF surface mapping of sulfate concentration on Michelangelo's David', *X-Ray Spectrometry* 35(5), 276–279.

Clark, B., Baird, A., Weldon, R., Tsusaki, D., Schnabel, L. and Candelaria, M. (1982), 'Chemical-Composition of Martian Fines', *Journal of Geophysical Research* 87(NB12), 59–67.

Cruz, N. and Matos, A. (2010), Adaptive sampling of thermoclines with autonomous underwater vehicles, *in* 'Proceedings - Oceans, 2010, Seattle, USA', pp. 1 –6.

Cruz, N., Matos, A., Martins, A., Silva, J., Santos, D., Boutov, D., Ferreira, D. and Pereira, F. (1999), Estuarine environment studies with Isurus, a REMUS class AUV, *in* 'Oceans, 1999, Seattle, USA', Marine Technol Soc; Ocean Engn Soc, Inst Elect & Electr Engn, pp. 1205–1210.

Davie, A., Hartmann, K., Timms, G., de Groot, M. and McCulloch, J. (2008), Benthic habitat mapping with autonomous underwater vehicles, *in* 'Proceedings - Oceans, 2008, Quebec City, Canada', pp. 1 –9.

de Souza, P. (1998), 'Advances in mossbauer data analysis', *Hyperfine Interactions* 113, 383–390. 10.1023/A:1012673027232.

de Souza, P., Davie, A., Timms, G., Butler, E. and Garg, V. (2010), Characterisation of suspended particles collected from an estuary in an urban and industrialised centre using magnets onboard an autonomous underwater vehicle, *in* 'Proceedings - Oceans, 2010, Sydney, Australia', pp. 1 –3.

Deslattes, R. D., Kessler, E. G., Indelicato, P., de Billy, L., Lindroth, E. and Anton, J. (2003), 'X-ray transition energies: new approach to a comprehensive evaluation', *Rev. Mod. Phys.* 75, 35–99.

Diankov, R. (2010), Automated Construction of Robotic Manipulation Programs, PhD thesis, Carnegie Mellon University, Robotics Institute.

Dunbabin, M., Roberts, J., Usher, K., Winstanley, G. and Corke, P. (2005), A hybrid auv design for shallow water reef navigation, *in* 'Proceedings - IEEE International Conference on Robotics and Automation, 2005, Barcelona, Spain', pp. 2105 – 2110.

EPA (2003), Surface-sediment sampling technologies, Technical report, U.S. Environmental Protection Agency, Cincinnati, Ohio.

Farrell, J., Li, W., Pang, S. and Arrieta, R. (2003), Chemical plume tracing experimental results with a REMUS AUV, *in* 'Proceedings - Oceans, 2003, San Diego, USA', Marine Technol Soc; IEEE; OES; Scripps Inst Oceanog, pp. 962–968.

Farrell, J., Pang, S., Li, W. and Arrieta, R. (2003), Chemical plume tracing experimental results with a remus auv, *in* 'Proceedings - Oceans, 2003, San Diego, USA', Vol. 2, pp. 962 –968 Vol.2.

Floyd, T. (1984), *Electronic devices*, Merril, Columbus, Ohio.

Fraser, G., Cesareo, R., Markowicz, A., Ramsey, M. H., Piorek, S., Liangquan, G. and Williams-Thorpe, O. (2008), *Portable X-ray Fluorescence Spectrometry: Capabilities for In Situ Analysis*, The Royal Society of Chemistry, Cambridge, UK.

Goldberg, D. E. (1989), *Genetic Algorithms in Search, Optimization and Machine Learning*, 1st edn, Addison-Wesley Longman Publishing Co., Inc., Boston, MA, USA.

Gould, J., Roemmich, D., Wijffels, S., Freeland, H., Ignaszewsky, M., Jianping, X., Pouliquen, S., Desaubies, Y., Send, U., Radhakrishnan, K. et al. (2004), 'Argo profiling floats bring new era of in situ ocean observations', *Eos* 85(19), 179–184.

Hagen, P. E., Storkersen, N., Marthinsen, B.-E., Sten, G. and Vestgard, K. (2008), 'Rapid environmental assessment with autonomous underwater vehicles - Examples from HUGIN operations', *Journal of Marine Systems* 69(1-2), 137–145.

Hartmann, K., de Souza, P., Timms, G. and Davie, A. (2009), Measuring light attenuation with a compact optical emission spectrometer and ctd mounted on a low cost auv, *in* 'Proceedings - Oceans, 2009, Bremen, Germany', pp. 1 –5.

Holland, J. H. (1975), *Adaptation in Natural and Artificial Systems*, The University of Michigan Press.

Hubbell, J. and Seltzer, S. (1995), Tables of x-ray mass attenuation coefficients and mass energy-absorption coefficients 1 kev to 20 mev for elements z= 1 to 92 and 48 additional substances of dosimetric interest, Technical report, National Inst. of Standards and Technology-PL, Gaithersburg, MD (United States). Ionizing Radiation Div.

Iborra, A., Pastor, J., Alvarez, B., Fernandez, C. and Merono, J. (2003), 'Robots in radioactive environments', *IEEE Robotics Automation Magazine* 10(4), 12 – 22.

III, P. T., Baird, A., Clark, B., Keil, K. and Jr., H. J. R. (1973), 'Inorganic chemical investigation by x-ray fluorescence analysis: The viking mars lander', *Icarus* 20(2), 153 – 178.

Janssens, K., Vittiglio, G., Deraedt, I., Aerts, A., Vekemans, B., Vincze, L., Wei, F., Deryck, I., Schalm, O., Adams, F., Rindby, A., Knochel, A., Simionovici, A. and Snigirev, A. (2000), 'Use of microscopic XRF for non-destructive analysis in art and archaeometry', *X-Ray Spectrometry* 29(1), 73–91.

Kalnicky, D. J. and Singhvi, R. (2001), 'Field portable XRF analysis of environmental samples', *Journal of Hazardous Materials* 83(12), 93 – 122.

King, P., Lewis, R., Walker, D., Alexander, P., Bose, N. and Worby, A. (2010), The memorial explorer: Developing the role of auvs in under-ice research, *in* 'Proceedings - Oceans, 2010, Sydney, Australia', pp. 1 –6.

Kirkwood, W. J. (2007), 'Development of the dorado mapping vehicle for multibeam, subbottom, and sidescan science missions', *Journal of Field Robotics* 24(6), 487–495.

Klencsár, Z. (1997), 'Mössbauer spectrum analysis by evolution algorithm', *Nuclear Instruments and Methods in Physics Research Section B: Beam Interactions with Materials and Atoms* 129(4), 527 – 533.

Knoll, G. F. (2010), *Radiation detection and measurement*, 4th edn, Wiley, New York :.

Lazic, V., Colao, F., Fantoni, R., Spizzichino, V. and Jovicevic, S. (2007), 'Underwater sediment analyses by laser induced breakdown spectroscopy and calibration procedure for fluctuating plasma parameters', *Spectrochimica Acta Part B: Atomic Spectroscopy* 62(1), 30–39.

Lechner, P., Eckbauer, S., Hartmann, R., Krisch, S., Hauff, D., Richter, R., Soltau, H., Stüder, L., Fiorini, C., Gatti, E., Longoni, A. and Sampietro, M. (1996), 'Silicon drift detectors for high resolution room temperature x-ray spectroscopy', *Nuclear Instruments and Methods in Physics Research Section A: Accelerators, Spectrometers, Detectors and Associated Equipment* 377(23), 346 – 351.

Leonard, N. E., Paley, D. A., Davis, R. E., Fratantoni, D. M., Lekien, F. and Zhang, F. (2010), 'Coordinated control of an underwater glider fleet in an adaptive ocean sampling field experiment in monterey bay', *Journal of Field Robotics* 27(6), 718–740.

Liu, F., Zhang, H. and Du, B. (2011), Design and optimization of overall structure for a landing auv, *in* 'Proceedings - International Conference on Mechatronics and Automation, 2011, Beijing, China', pp. 1345 –1349.

LocoSys (2012), 'LS20031 GPS Smart Antenna'. `http://www.locosystech.com/product.php?zln=en&id=20`.

Luo, L., Chettle, D. R., Nie, H., McNeill, F. E. and Popovic, M. (2006), 'Curve fitting using a genetic algorithm for the x-ray fluorescence measure-

ment of lead in bone', *Journal of Radioanalytical and Nuclear Chemistry* 269, 325–329.

Mantler, M. and Schreiner, M. (2000), 'X-ray fluorescence spectrometry in art and archaeology', *X-Ray Spectrometry* 29(1), 3–17.

Matos, A., Cruz, N., Martins, A. and Lobo Pereira, F. (1999), Development and implementation of a low-cost lbl navigation system for an auv, *in* 'Proceedings - Oceans, 1999, Seattle, USA'.

Michel, A., Farr, N. and Chave, A. (2006), Evaluation of laser-induced breakdown spectroscopy (libs) as a new in situ chemical sensing technique for the deep ocean, *in* 'Proceedings - Oceans, 2006, Boston, USA', pp. 1 –5.

MicroStrain-Sensing-Systems (2012), '3dm-gx1'. `http://www.microstrain.com/inertial/3DM-GX1`.

Moioli, P. and Seccaroni, C. (2000), 'Analysis of art objects using a portable x-ray fluorescence spectrometer', *X-Ray Spectrometry* 29(1), 48–52.

OceanServer (2012), 'Oceanserver digital compass'. `http://www.ocean-server.com/compass.html`.

Pala, C. (2013), 'Giant marine reserves pose vast challenges', *Science* 339(6120), 640–641.

Pichahchy, A., Cremers, D. and Ferris, M. (1997), 'Elemental analysis of metals under water using laser-induced breakdown spectroscopy', *Spectrochimica Acta Part B: Atomic Spectroscopy* 52(1), 25–39.

Popa, D., Sanderson, A., Komerska, R., Mupparapu, S., Blidberg, D. and Chappel, S. (2004), Adaptive sampling algorithms for multiple autonomous underwater vehicles, *in* 'Proceedings - Oceans, 2004, Sebasco, USA', IEEE; OES, pp. 108–118.

Purcell, M., von Alt, C., Allen, B., Austin, T., Forrester, N., Goldsborough, R. and Stokey, R. (2000), New capabilities of the REMUS autonomous

underwater vehicle, *in* 'Proceedings - Oceans, 2000, Providence, USA', Marine Technol Soc; IEEE; OES, pp. 147–151.

Rieder, R., Gellert, R., Bruckner, J., Klingelhofer, G., Dreibus, G., Yen, A. and Squyres, S. (2003), 'The new Athena alpha particle X-ray spectrometer for the Mars Exploration Rovers', *Journal of Geophysical Research - Planets* 108(E12).

Rieder, R., Wanke, H., Economou, T. and Turkevich, A. (1997), 'Determination of the chemical composition of Martian soil and rocks: The alpha proton X ray spectrometer', *Journal of Geophysical Research - Planets* 102(E2), 4027–4044.

Robinson, R., Davie, A. and de Souza, P. (2010), Extracting valuable information from a simultaneous visualisation of science and engineering data obtained with an autonomous underwater vehicle, *in* 'Proceedings - Oceans, 2010, Sydney, Australia', pp. 1 –5.

Rousseau, R. M. (2006), 'Corrections for matrix effects in x-ray fluorescence analysisa tutorial', *Spectrochimica Acta Part B: Atomic Spectroscopy* 61(7), 759 – 777.

Salles, E., de Souza, P. and Garg, V. (1995), 'Identification of crystalline structures using mössbauer parameters and artificial neural network', *Journal of Radioanalytical and Nuclear Chemistry* 190, 439–447. DOI: 10.1007/BF02040024.

San-Jose-Technology (2012), 'Fv-m8'. `http://www.sanav.com/gps_engine_board/FV-M8.htm`.

Sangekar, M., Thornton, B., Nakatani, T., Bodenmann, A., Sakamaki, T. and Ura, T. (2011), Autonomous landing experiments with an underwater vehicle for multi-resolution wide area seafloor observation, *in* 'Proceedings - Oceans, 2011, Waikoloa, USA', pp. 1 –7.

Sangekar, M., Thornton, B., Nakatani, T. and Ura, T. (2010), Development of a landing algorithm for autonomous underwater vehicles using laser profiling, *in* 'Proceedings - Oceans, 2010, Sydney, Australia', pp. 1 –7.

Sarrazin, P., Blake, D., Feldman, S., Chipera, S., Vaniman, D. and Bish, D. (2005), 'Field deployment of a portable X-ray diffraction/X-ray flouresence instrument on Mars analog terrain', *Powder Diffraction* 20(2), 128–133.

Schofield, O., Kohut, J., Aragon, D., Creed, L., Graver, J., Haldeman, C., Kerfoot, J., Roarty, H., Jones, C., Webb, D. and Glenn, S. (2007), 'Slocum gliders: Robust and ready', *Journal of Field Robotics* 24(6), 473–485.

Shackley, S. (2010), *X-Ray Fluorescence Spectrometry (XRF) in Geoarchaeology*, Springer Dordrecht Heildelberg London.

Singh, S., Webster, S., Freitag, L., Whitcomb, L., Ball, K., Bailey, J. and Taylor, C. (2009), Acoustic communication performance of the whoi micromodem in sea trials of the nereus vehicle to 11,000 m depth, *in* 'Proceedings - Oceans, 2009, Biloxi, USA', pp. 1 –6.

Smith, D. and Dunbabin, M. (2007), Automated counting of the northern pacific sea star in the derwent using shape recognition, *in* 'Proceedings - 9th Biennial Conference of the Australian Pattern Recognition Society on Digital Image Computing Techniques and Applications, 2007, Glenelg, Australia', pp. 500 –507.

Smith, S., An, P., Holappa, K., Whitney, J., Burns, A., Nelson, K., Heatzig, E., Kempfe, O., Kronen, D., Pantelakis, T., Henderson, E., Font, G., Dunn, R. and Dunn, S. (2001), 'The morpheus ultramodular autonomous underwater vehicle', *Oceanic Engineering, IEEE Journal of* 26(4), 453 – 465.

Squyres, S. W., Knoll, A. H., Arvidson, R. E., Ashley, J. W., Bell, J. F., Calvin, W. M., Christensen, P. R., Clark, B. C., Cohen, B. A., de Souza, P. A., Edgar, L., Farrand, W. H., Fleischer, I., Gellert, R., Golombek, M. P., Grant, J., Grotzinger, J., Hayes, A., Herkenhoff, K. E., Johnson, J. R., Jolliff, B., Klingelhöfer, G., Knudson, A., Li, R., McCoy, T. J., McLennan, S. M., Ming, D. W., Mittlefehldt, D. W., Morris, R. V., Rice, J. W., Schröder, C., Sullivan, R. J., Yen, A. and Yingst, R. A. (2009),

'Exploration of victoria crater by the mars rover opportunity', *Science* 324(5930), 1058–1061.

SSI-Technologies (2012), 'Pressure sensors'. http://www.ssi-sensors.com/wp/pressure-sensors/.

Stallard, M., Apitz, S. and Dooley, C. (1995), 'X-ray fluorescence spectrometry for field analysis of metals in marine sediments', *Marine Pollution Bulletin* 31(412), 297 – 305.

Stojanovic, M. (1996), 'Recent advances in high-speed underwater acoustic communications', *IEEE Journal of Oceanic Engineering* 21(2), 125 –136.

Stutters, L., Liu, H., Tiltman, C. and Brown, D. (2008), 'Navigation technologies for autonomous underwater vehicles', *IEEE Transactions on Systems, Man, and Cybernetics, Part C: Applications and Reviews* 38(4), 581 –589.

Szokefalvi-Nagy, Z., Demeter, I., Kocsonya, A. and Kovacs, I. (2004), 'Non-destructive XRF analysis of paintings', *Nuclear Instruments and Methods in Physics Research Section B: Beam Interactions with Materials and Atoms* 226(1-2), 53–59.

Thompson, D. (2007), AUV Operations at MBARI, *in* 'Proceedings - Oceans, 2007, Vancouver, Canada', pp. 1 –6.

Tritech (2012), 'Pa500 digital precision altimeter'. http://www.tritech.co.uk/product/tritech-pa200-pa500.

USGlobalSat (2012), 'Em-408'. www.usglobalsat.com/p-47-em-408-sirf-iii.aspx.

Van Grieken, R. and Markowicz, A. (2001), *Handbook of X-Ray Spectrometry, Second Edition,*, Practical Spectroscopy, Taylor & Francis.

Vaniman, D., Bish, D., Blake, D., Elliott, S., Sarrazin, P., Collins, S. and Chipera, S. (1998), 'Landed XRD/XRF analysis of prime targets in the search for past or present Martian life', *Journal of Geophysical Research - Planets* 103(E13), 31477–31489.

Vekemans, B., Janssens, K., Vincze, L., Adams, F. and Van Espen, P. (1994), 'Analysis of x-ray spectra by iterative least squares (axil): New developments', *X-Ray Spectrometry* 23(6), 278–285.

von Alt, C., Allen, B., Austin, T., Forrester, N., Goldsborough, R., Purcell, M. and Stokey, R. (2001), Hunting for mines with REMUS: A high performance, affordable, free swimming underwater robot, *in* 'Proceedings - Oceans, 2001, Honolulu, USA', Marine Technol Soc; IEEE; OES; Minerals, Met & Mat Soc; Soc Explorat Geophysicists; Amer Geophys Union; Womens Aquat Network; Coasts, Oceans, Ports & Rivers Inst; Amer Meteorol Soc; Oceanog Soc, pp. 117–122.

Wang, S., Zhang, H., Hou, W. and Liang, J. (2007), 'Control and navigation of the variable buoyancy auv for underwater landing and takeoff', *International Journal of Control* 80(7), 1018–1026.

West, M. and Syrmos, V. (2006), Navigation of an autonomous underwater vehicle(auv) using robust slam, *in* 'Computer Aided Control System Design, 2006 IEEE International Conference on Control Applications, 2006 IEEE International Symposium on Intelligent Control, 2006 IEEE', pp. 1801–1806.

Wettergreen, D., Thorpe, C. and Whittaker, R. (1993), 'Exploring mount erebus by walking robot', *Robotics and Autonomous Systems* 11(34), 171 – 185.

Whitehead, J., Coughanowr, C., Agius, J., Chrispijn, J., Taylor, U. and Wells, F. (2009), *State of the Derwent Estuary: a review of pollution sources, loads and environmental quality data from 2003 to 2009*, Derwent Estuary Program, Department of Primary Industries, Water and Environment, Hobart, Tas.

Wogman, N. and Nielson, K. (1980), 'Development and application of an in situ x-ray fluorescence spectrometer for underwater sediment analysis', *Environment International* 4(4), 313 – 324.

Wogman, N., Rieck, H. and Kosorok, J. (1975), 'In situ analysis of sedimentary pollutants by x-ray fluorescence', *Nuclear Instruments and Methods* 128(3), 561 – 568.

Wright, A. H. (1991), Proceedings - genetic algorithms for real parameter optimization, 1991, indiana, usa, *in* 'Foundations of Genetic Algorithms', Morgan Kaufmann, pp. 205–218.

Yuh, J. and West, M. (2001), 'Underwater robotics', *Advanced Robotics* 15(5), 609–639.

Zhang, Y., McEwen, R., Ryan, J. and Bellingham, J. (2010), 'Design and tests of an adaptive triggering method for capturing peak samples in a thin phytoplankton layer by an autonomous underwater vehicle', *Oceanic Engineering, IEEE Journal of* 35(4), 785 –796.

Zielinski, A., Yoon, Y.-H. and Wu, L. (1995), 'Performance analysis of digital acoustic communication in a shallow water channel', *IEEE Journal of Oceanic Engineering* 20(4), 293 –299.

Appendix A

Theory of X-Ray Fluorescence Spectrometry

This appendix provides some more detailed theory pertaining to the topic of XRF spectroscopy.

When an X-ray strikes a material it can either be scattered or absorbed by the material's constituent atoms. In the absorption scenario, if the incident X-ray is of sufficient energy it can cause an electron to be emitted from the atom. This process is known as the photoelectric effect and is shown in Figure A.1.

The ejected electrons can be from the inner shells (energy E_0) in the atom. This creates vacancies, resulting in the atom being in an excited state. In order to return to a stable state an electron belonging to a higher energy (energy E_j) shell drops down to fill the vacancy. This is shown in Figures A.2 and A.3. When this occurs, the energy difference ($E_{tot} = E_j$ - E_i) between the two shells is emitted as a characteristic X-ray. Each element has a unique set of energy levels. Therefore the energy of the emitted characteristic X-ray is unique to the element that produced it.

Each energy shell in an atom is given a designation. From the inner most shell outwards they are known as K, L, M, N etc. These labels are also used in identifying the origin of the characteristic X-rays. For example a K X-ray is produced through the ejection of an electron from the K shell. A

further designation, α, β or γ, indicates from which shell the electron which fills the vacancy originates from. Figures A.2 and A.3 provide an example of characteristic X-ray labelling using a zinc atom. Within each energy level there are additional orbitals. A subscript is used to denote from which orbital the electron originated (α_1, α_2, β_1, β_2).

A competing process is when the energy difference is instead transferred to an outer shell electron, causing it to be ejected from the atom instead of an X-ray. This is known as the Auger effect.

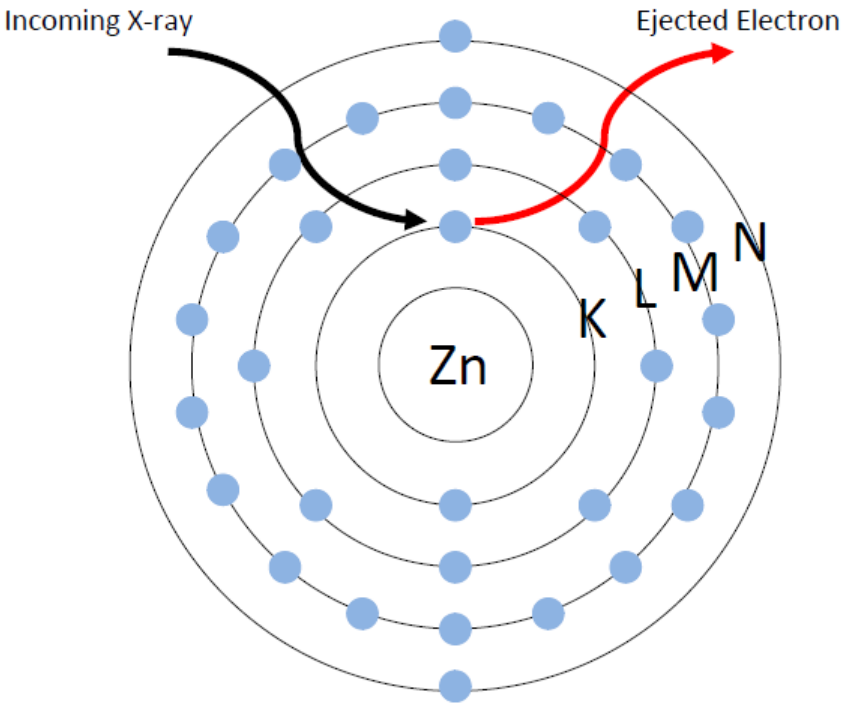

Figure A.1: An atom of zinc being struck by an X-ray of sufficient energy to eject an electron from the K shell.

Through detection and measurement of an X-ray's energy it is possible to identify the element that produced it. X-ray intensity increases with the concentration of a particular element within a sample.

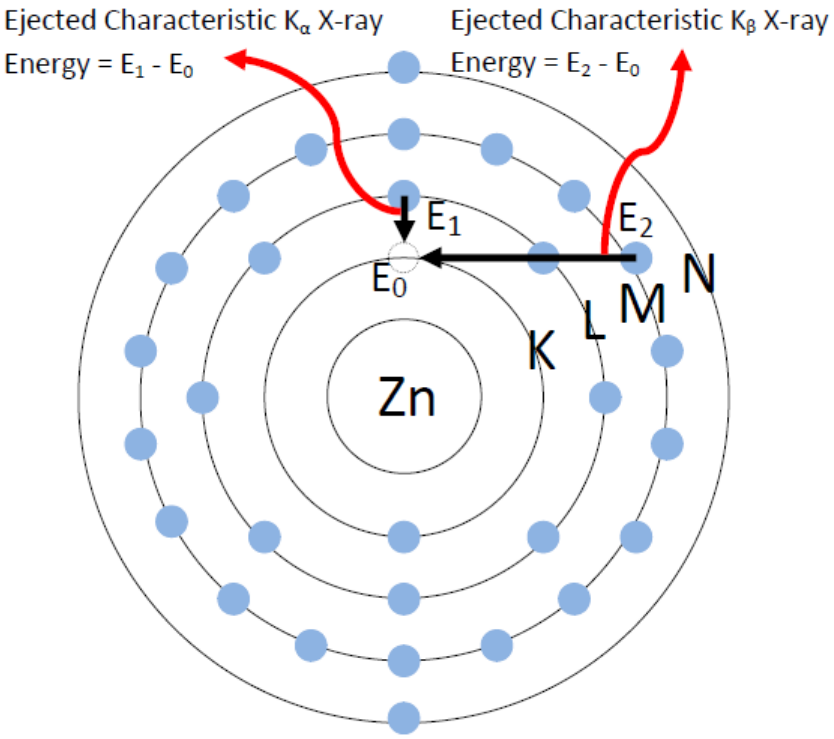

Figure A.2: An electron from either the L or M shell moves down to fill the vacancy in the K shell. A characteristic X-ray is emitted from the atom with energy equal to the energy difference in shells and are known as K X-rays.

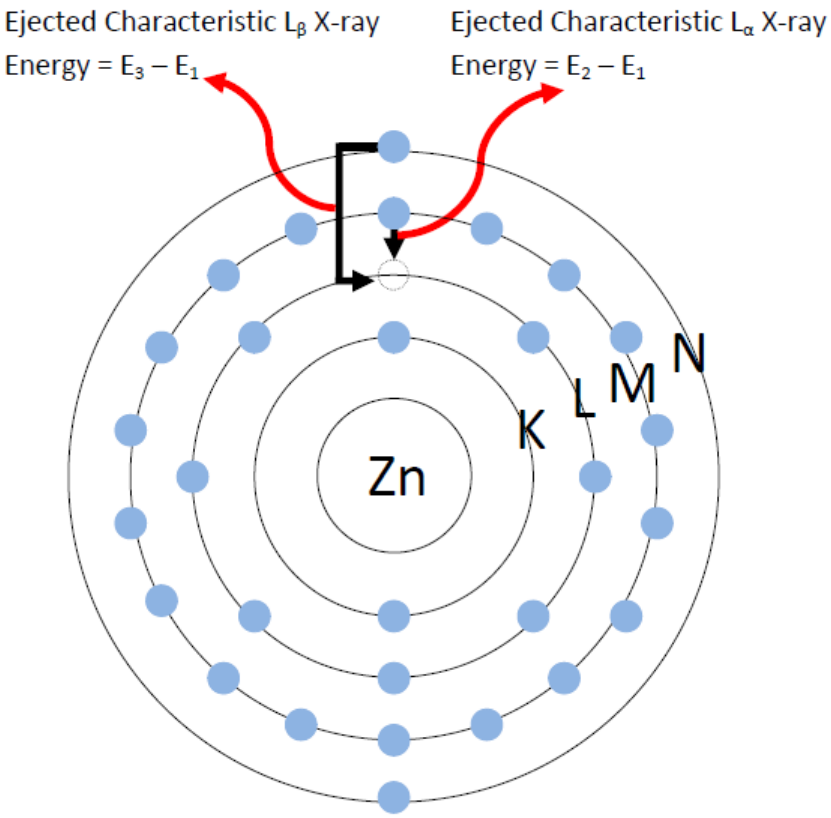

Figure A.3: When a vacancy is present in the L shell then electrons from either the M or N shells move down to fill the void. The resulting characteristic X-ray is known as an L X-ray.

The intensity of characteristic X-rays is given by:

$$(I_i) = G\frac{\epsilon(E_i)a_i(E_0)I_0(E_0)}{sin\Psi_1} \times \frac{1 - exp[-\rho T(\mu(E_0)csc\Psi_1 + \mu(E_i)csc\Psi_2)]}{\mu(E_0)csc\Psi_1 + \mu(E_i)csc\Psi_2} \tag{A.1}$$

with:

$$a_i = C_i\tau_i(E_0)\omega_i p_i(1 - \frac{1}{j_i}) \tag{A.2}$$

where Ψ_1 and Ψ_2 are the incidence and takeoff angles, G is a measurement geometry factor, $\epsilon(\mathrm{E}_i)$ is the efficiency of the detector to detect X-rays of energy E_i, ρ is the density of the sample, $\mu(\mathrm{E}_0)$ and $\mu(\mathrm{E}_i)$ are the total mass attenuation coefficients of the primary and characteristic radiation in the whole sample, $\mathrm{I}_0(\mathrm{E}_0)$ is the number of photons of primary radiation per second, C_i is the concentration of the element in the analysed sample, T is the thickness of the sample and $\tau_i(\mathrm{E}_0)$ is the photoelectric mass absorption coefficient of element i.

This equation is modified by the presence of an enhancement effect caused by other elements in the excited sample. The increase in intensity is due to the characteristic X-rays of other elements exciting the element i. This increase is given by an enhancement term, H_i.

$$\begin{aligned} H_i = {} & \frac{1}{2\mu_i(E_0)} \sum_{k=1}^{m} C_k\omega_k(1 - \frac{1}{j_k})\mu_i(E_k)\mu_k(E_0)\times \\ & [\frac{(ln(1 + \mu(E_0)/[\mu(E_k)sin\Psi_1])}{\mu(E_0)/sin\Psi_1} + \frac{ln(1 + \mu(E_i)/[\mu(E_k)sin\Psi_2])}{\mu(E_i)/sin\Psi_2}] \end{aligned} \tag{A.3}$$

where $\mu_i(\mathrm{E}_0)$ and $\mu_i(\mathrm{E}_k)$ are the total mass attenuation coefficients for the element i at energy E_0 and at the characteristic X-ray energy of element k, $\mu_k(\mathrm{E}_0)$ is the total mass attenuation coefficient for element k at the energy E_0, $\mu(\mathrm{E}_0)$ is the total mass attenuation coefficient for the whole sample at energy E_0 and m is the total number of elements in the sample.

The presence of this enhancement term, and also the dependence of the

intensity on the total mass attenuation coefficient of the whole sample at the primary energy and the characteristic energy in Equation A.1, indicates that the characteristic energy intensity for a particular element is dependent on the makeup up of the whole sample. This dependence is known as the matrix effect.

Equation A.1 can be simplified depending on whether the sample can be classified as a thin sample or a thick sample. If the mass per unit area of the sample is sufficiently small, then the sample can be referred to as thin. In this case, the equation becomes

$$(I_i)_{thin} = K_i m_i \tag{A.4}$$

where K_i is a calibration factor and m_i is the mass per unit area of the ith element. This simplification is valid for cases where the total mass per unit area of the sample satisfies the following conditions:

$$m_{thin} \leq \frac{0.1}{\mu(E_0)csc\Psi_1 + \mu(E_i)csc\Psi_2} \tag{A.5}$$

The intensity of characteristic X-rays for the thin samples is linearly dependent on the mass per unit area of the element meaning that the matrix effects can be neglected.

A thick sample is one where the mass per unit area is greater than what is known as the saturation mass. This is the mass above which no further increase in characteristic X-ray intensity is observed. This time Equation A.1 simplifies to

$$(I_i)_{thick} = \frac{G\epsilon(E_i)a_i(E_0)I_0(E_0)}{\mu(E_0) + (sin\Psi_1/sin\Psi_2)\mu(E_i)} \tag{A.6}$$

This holds as long as the mass per unit area of the sample satisfies the conditions:

$$m_{thick} \leq \frac{4.61}{\mu(E_0)csc\Psi_1 + \mu(E_i)csc\Psi_2} \tag{A.7}$$

This is the equation that is relevant to the emission of characteristic X-rays that will be encountered in analysis of marine sediments.